



DEGREE PROJECT IN ELECTRIC POWER ENGINEERING 120 CREDITS,
SECOND CYCLE

STOCKHOLM, SWEDEN 2015

Feeder Dynamic Rating Application for Active Distribution Networks using Synchrophasors

NARENDER SINGH

KTH ROYAL INSTITUTE OF TECHNOLOGY

SCHOOL OF ELECTRICAL ENGINEERING

KTH ROYAL INSTITUTE OF TECHNOLOGY

KTH Royal Institute of Technology

School of Electrical Engineering

Electric Power System (EPS) Department

Author: Narender Singh

Email Address: nsingh@kth.se

Study Program: Master in Electric power Engineering, 120 Credits

Supervisor: Dr. Luigi Vanfretti, Dr. Hossein Hooshyar

Abstract

There is an ever increasing demand of electricity and to meet this demand, installation of new transmission and distribution lines is required. This task requires a significant investment and consent from the respective authorities. An alternative is to utilize maximum capability of the existing lines. Static line ratings are based on a conservative estimate, which means that on most occasions, the actual capacity of lines is much higher than the static line ratings.

In order to provide a solution to this problem, this thesis introduces an approach that has been developed to utilize real time weather conditions, conductor sag data and the actual line loading of the conductor from PMU to provide dynamic line ratings for active distribution networks. The application has been developed in LabVIEW environment which provides a user friendly front panel where real-time ampacity can be seen as a waveform while being compared to the actual line loading.

The developed application has been tested on the reference grid created for IDE4L project. The ampacity calculation method introduced here makes use of real-time data available through a real-time simulator in SmarTS lab at KTH, Sweden.

Keywords

Ampacity, Dynamic line rating, IEEE 738-2006, Kalman filter, LabVIEW, Line loading, Opal-RT, PMU, State change equation

Sammanfattning

Det är ett ökande behov av elektricitet och för att möta detta behovet, installation av nya transmission och distributionsledningar behövs. Denna utbyggnad kräver ett stort engagemang och förståelse från ansvariga grupper. Ett alternativ är att utnyttja max-kapaciteten på redan befintliga ledningar. Installerade ledningar har räknats på ett konservativt sätt, vilket innebär att det vid vissa tillfällen går att öka belastningen på dessa. För att ge en lösning på detta problem, introducerar den här avhandlingen en metod för att använda realtids-väderdata, tabeller för ledningarnas utvidgning och realtids-belastningsdata från PMU för att framställa dynamisk data för aktiva distributions-nätverk. Applikationen har utvecklats i LabVIEW-miljön som har ett användarvänligt GUI, där "Real-time ampacity" kan ses som en vågform medans den jämförs mot den faktiska belastningen på ledningen. Den utvecklade applikationen har testats på referens-miljön som skapats för IDE4L projektet. "Ampacity calculation metoden" som introduceras här använder sig av realtidsdata som görs tillgänglig igenom en realtids-simulator i SmarTSlab på Kungliga Tekniska Högskolan i Sverige.

Acknowledgements

I express sincere gratitude to Dr. Hossein Hooshyar for giving me this thesis topic in the first place and for his support, motivation and patience throughout my thesis work. He has been an ideal supervisor.

I would like to thank Dr. Luigi Vanfretti who with his immense knowledge guided me with good advice all through my thesis work.

I am thankful to all the members of SmarTS Lab for helping me out in different ways during my thesis.

Finally, I thank my family for their unconditional love and support.

Table of Contents

1	Introduction.....	1
1.1	Background	1
1.2	Real-time data acquisition	2
1.3	Dynamic line ratings in distribution systems	2
1.4	Objectives.....	6
1.4.1	General objectives.....	6
1.4.2	Specific objectives.....	6
1.5	Organization of thesis chapters and description.....	6
2	Literature Review and theory development	9
2.1	Problem definition.....	9
2.2	Static ratings	9
2.3	Dynamic line rating techniques	10
2.3.1	Weather dependent systems	10
2.3.2	Temperature dependent systems.....	10
2.3.3	Tension monitoring systems	11
2.3.4	Sag dependent systems.....	12
2.3.5	Distributed temperature sensing	13
2.3.6	Object oriented power line ampacity system	13
2.4	Algorithm for real-time dynamic feeder rating.....	14
3	IEEE 738 standard for calculating the current-temperature of bare overhead conductors.....	17
3.1	Term definitions	17
3.1.1	Conductor temperature.....	17
3.1.2	Heat capacity	18
3.1.3	Reynolds number	18
3.1.4	Specific heat.....	18
3.2	Calculations	18
3.2.1	Steady state calculations	18
3.2.2	Transient calculations	19
3.2.3	Time-varying weather and current calculations.....	20
3.3	Symbols and Description	20
3.4	Formulas.....	22
3.4.1	Steady state heat balance.....	22
3.4.2	Non-steady state heat balance	22
3.4.3	Convection heat loss rate	22
3.4.4	Natural convection.....	23
3.4.5	Radiated heat loss rate.....	23
3.4.6	Rate of solar heat gain	23
3.4.7	Conductor electrical resistance	23
3.4.7.1	<i>Skin effect.....</i>	<i>24</i>
3.4.8	Equations for air properties, solar angles and solar flux.....	24
3.4.8.1	<i>Dynamic viscosity of air</i>	<i>25</i>
3.4.8.2	<i>Air density.....</i>	<i>25</i>
3.4.8.3	<i>Thermal conductivity of air.....</i>	<i>25</i>
3.4.9	Altitude of the sun.....	25
3.4.10	Azimuth of sun	25
3.4.11	Total heat flux received by a surface at sea level.....	26
3.4.12	Total heat flux elevation correction factor	26
3.5	Use of the standard in algorithm	26
3.5.1	To calculate conductor temperature.....	27

3.5.2	Ampacity calculation.....	27
4	State change equation	29
4.1	Formulas.....	29
4.2	Determination of specific wind load	31
4.3	Sag measurement method.....	32
4.3.1	Sag level monitoring.....	33
4.3.2	Ruling span sag.....	33
5	Kalman filter.....	35
5.1	Implementation and effect of Kalman filter	36
6	Instrumentation and data acquisition.....	39
6.1	SmarTS lab architecture	39
6.2	Application process	39
6.2.1	Reference grid.....	40
6.2.2	Opal RT simulator	41
6.2.3	Phasor Measurement Unit.....	42
6.2.4	Phasor Data Concentrators	42
6.2.5	PMU connection tester	43
6.3	S³DK.....	44
6.4	Real-time weather data.....	46
6.5	LabVIEW application.....	47
6.5.1	Auto-generated report	49
7	Testing and Results	51
7.1	Test model.....	51
7.2	Results.....	53
7.2.1	Impact of weather, line loading and sag on line ampacity	53
7.2.2	Impact of weather variation	54
8	Conclusion and future work.....	57
8.1	Conclusion.....	57
8.2	Future work.....	58
	BIBLIOGRAPHY	59
	Appendix A.....	63
	Appendix B.....	73

List of Figures

Figure 1.1 PMU to PDC flow	2
Figure 2.1 Power Donut	11
Figure 2.2 Tension monitoring system	12
Figure 2.3 Sag-monitoring system	12
Figure 2.4 DTS using Raman scattering.....	13
Figure 2.5 Block diagram of real-time ampacity estimation algorithm	14
Figure 3.1 Steady state conductor temperature	19
Figure 3.2 Step change.....	19
Figure 4.1 Line sag	32
Figure 4.2 GPS device placement	32
Figure 4.3 Sag alarm triggering algorithm	33
Figure 5.1 Operation of a Kalman filter	35
Figure 5.2 Kalman filter implementation.....	36
Figure 5.3 Kalman filter effect	37
Figure 6.1 SmarTS Lab architecture.....	39
Figure 6.2 Application process block diagram	40
Figure 6.3 Reference Grid SIMULINK model.....	40
Figure 6.4 Opal RT Simulator	41
Figure 6.5 SEL-421	42
Figure 6.6 BRK37M board.....	42
Figure 6.7 Synchrophasor data collection network.....	43
Figure 6.8 SEL-5073 Synchrowave output	43
Figure 6.9 PMU connection tester.....	44
Figure 6.10 S3DK interface.....	45
Figure 6.11 S3DK activation.....	45
Figure 6.12 Configuration.....	45
Figure 6.13 Running S3DK.....	45
Figure 6.14 Buffer and Queue, Bad Data, Advanced.....	45
Figure 6.15 S3DK Channel Selector.....	46
Figure 6.16 Application for receiving weather data	47
Figure 6.17 LabVIEW application	48
Figure 7.1 Reference grid model.....	51
Figure 7.2 Medium voltage part of reference grid.....	52
Figure 7.3 Impact of weather, line loading and sag on line ampacity	53
Figure 7.4 Impact of weather variation	54
Figure A.1-A.8 Ambient temperature January 2015- August 2015.....	63
Figure A.9-A.16 Wind speed January 2015- August 2015.....	66
Figure A.17-A.24 Solar radiation January 2015- August 2015.....	69

List of Tables

Table 1.1 Different DLR techniques and cost analysis	5
Table 2.1 Inputs required for the method and their source	15
Table 3.1: Symbol, Description and SI units	20
Table 3.2: Solar azimuth constant.....	26
Table 3.3: Coefficient values in clear and industrial atmosphere.....	26
Table 4.1: ACSR data	30
Table 4.2: Conductor parameters.....	31
Table 4.3: Dynamic pressure coefficient	31
Table 4.4: Line data for IEEE 34-bus feeder.....	34
Table 6.1: Simulator specifications.....	41
Table 6.2 Auto-generated report	49
Table 7.1: Overhead line configuration	52

List of Acronyms

DG	Distributed Generation
DLR	Dynamic Line Rating
DTS	Distributed Temperature Tensing
GPS	Global Positioning System
GUI	Graphical User Interface
HIL	Hardware in the Loop
IEEE	Institute of Electrical and Electronics Engineers
LL	Line to Line
LTE	Long Term Emergency
MSEK	Millions Swedish Krona
PDC	Phasor Data Concentrator
PMU	Phasor Measurement Unit
STE	Short Term Emergency

Chapter 1

1 Introduction

There has been a consistent increment in electricity demand and it is not expected to stabilize or decline anytime in near future. Also, with increasing environmental concerns there has appeared a need not only to use environment friendly power resources but also to utilize the existing system to the highest possible capacity [1]. Another reason to make optimal use of existing resources is that transmission and distribution network extension requires consent from the authorities and a significant investment; this can take several years to be implemented. As a result electric utilities are under pressure to make optimum use of existing facilities [2]. On the other hand, monitoring “rating vs loading” of the feeders in active distribution networks is a critical task as the bi-directional power flow (due to presence of DGs) can cause the feeders to be easily overloaded.

1.1 Background

Dynamic line rating (DLR) is a tool to make optimal use of the power transmission and distribution channel. It is a method of power carriage optimization of transmission and distribution lines based not only on the current passing through them but the effects caused by factors such as wind speed, wind direction, solar radiation and ambient temperature are also acknowledged [3]. According to U.S Department of energy, all transmission owners and operators calculate static ratings for their lines for normal, long-term emergency (LTE), and short-term emergency (STE) conditions. The static rating, indicate the maximum amount of current that the conductor can carry without damaging the conductor. These ratings are based on worst-case scenario (low wind speed, high ambient temperature and high solar radiation) [4].

On the other hand, the dynamic thermal rating of overhead conductor may be defined as the conductor current that produce maximum allowable conductor temperature at a specific location and time along the power line [5]. These ratings are based on real time information which includes the ambient temperature, wind speed, wind direction, etc.

According to a study reported in [6], ampacity upgradation using DLR systems have shown to return annual benefit of 0.29 MSEK/GWh as compared to conductor upgrading and new line construction which give economic benefit of 0.14 MSEK/GWh and 0.09 MSEK/GWh respectively.

There have been significant developments in the field of DLR as a result of which relatively inexpensive, reliable and accurate instruments have become available to measure weather, transmission line sag-tension and conductor temperature. Data from these devices can be easily accessed through communication devices which transmit in real-time [7].

The main idea behind these methods is to somehow calculate the conductor's actual temperature using the available data like ambient data and conductor sag, etc. A standard method which can be used to calculate the permissible current through a conductor with the knowledge of conductor constants and ambient weather data in addition to conductor temperature is given in [8].

Dynamic ratings offer two key benefits over traditional static ratings [7]:

1. Higher loading of equipment is usually possible using actual measured load and weather parameters. Traditional static ratings are overly conservative, since they are based on worst-case weather and load assumptions.
2. A better understanding of equipment thermal response is achieved. This results in increased reliability.

1.2 Real-time data acquisition

A phasor measurement unit (PMU) is a device that provides real-time measurements of electrical quantities across the power system at a high sampling frequency. The phasor measurements are time stamped to a very accurate GPS clock. These PMUs can be placed at several different location in the power system to give a thorough overview of the entire system under supervision.

Measurements from the PMUs are time aligned by the means of phasor data concentrator (PDC) which receives measurement streams from multiple PMUs. Data from one PDC can be shared with other PDCs deployed in different locations. Multiple layers of concentration can be implemented within a lone synchrophasor data system.

Figure 1.1 shows the data flow from PMUs to PDC and thereafter, to the applications utilizing this data.

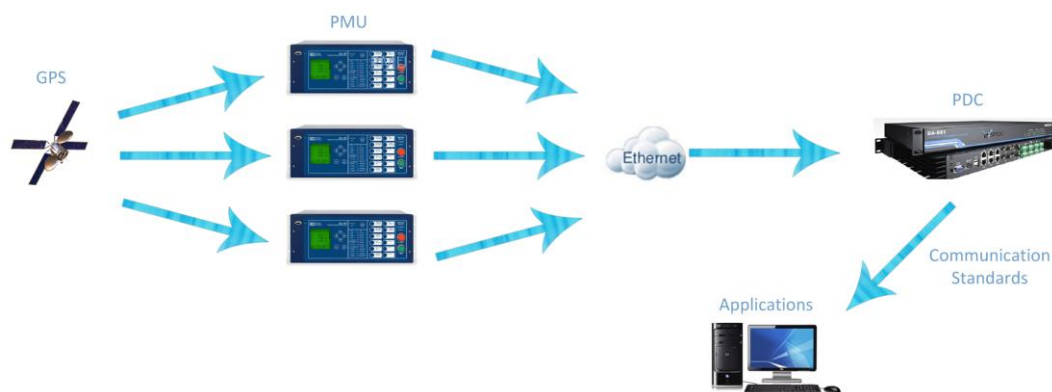


Figure 1.1 PMU to PDC flow

1.3 Dynamic line ratings in distribution systems

For the most part, the study and research conducted in the field of DLR has been focused on transmission part of the power system. This has left the area of distribution systems with a significant potential for research. Hence, in the same line this thesis has developed an approach for DLR estimation of overhead lines in the distribution system.

Based on the voltage level of the lines the distribution system can be subdivided into medium voltage and low voltage parts.

In North America medium voltage system consists of line to line voltages level: 4.6 kV, 12.0 kV, 12.47 kV, 13.2 kV, 13.8 kV, 21.6 kV, 22 kV, 24.9 kV, 34.5kV and 69 kV and low voltage: for single-phase 120 V LN and 240 V LL, and for three-phase 208 V and 480 V. On the other hand in Europe the medium voltage levels are: 6.6 kV, 10 kV, 11 kV, 12 kV, 15 kV, 20 kV, and 36 kV and low voltage levels for single-phase 230 V LN and for three-phase 400V.

These distribution systems are different from transmission systems. Line transposition is uneconomic and sometimes physically impossible in distribution systems. Also, the individual phase load levels are always changing due to which perfect balance is never achieved [9]. Phase loads depend on various factors like customer usage routine and weather conditions; this makes imbalance an inherent factor in distribution a network. As a literature review for developing an algorithm suitable for DLR system for distribution networks, many DLR systems have been studied. This section of the thesis is an analysis of these systems and their possible use in distribution network DLR.

The study reported in [10] uses PMU measurements to estimate line temperature and sag for a transmission line. The PMU data (positive sequence currents and voltages) at both ends of the line is used to derive positive sequence impedance, this impedance is then used to estimate the value of conductor temperature. Although this is an interesting method which makes use of PMU data for DLR estimation, this method cannot be utilized in the algorithm developed for this thesis. The reason being that for the distribution systems, positive sequence is irrelevant. The load on different phases can be and is mostly uneven which renders the approach in [10] irrelevant for this thesis work.

Also in [10], the author has introduced a method of conductor temperature based solely upon its resistance. In order to calculate the conductor temperature a suitable method is provided in [8]. This method accurately takes in to account the conductor temperature as a function of convection heat loss, radiated heat loss, solar heat gain and resistance of conductor temperature.

In [11], a device is introduced which is mounted directly on the line and it directly measures the conductor surface temperature. This device provides reasonable accuracy but this device will be uneconomic as unlike a transmission system, a distribution system has unbalanced phases and hence unequal temperatures which will require individual devices for each phase.

In [12], a dynamic line rating method is introduced in which a special device called Telemetric Monitoring of Temperature (TMT) has been developed. This device is a specialized unit to measure the conductor current and temperature of an overhead line. The measured conductor temperature and current are then transmitted through a telephony channel to the receiver. Although this method is efficient, it is not suitable for a distribution network. This is due to the fact that the range of conductor current that can be measured by this device is 250 A to 2000 A whereas in a distribution network the line current can be much lower.

A method for DLR estimation based solely upon PMU measurements is proposed in [13]. This method eliminates the need of installing any additional

equipment in the network which makes it an economic approach. This method has been designed to be used in a transmission network and it cannot be adapted for a distribution network due to two main reasons. Firstly, this method utilizes the relationship between positive sequence phasors of current and voltage signals to estimate the conductor temperature. And secondly, this method does not acknowledge the effect of ambient weather conditions on conductor temperature which have a significant impact on temperature.

In [14], a method of DLR estimation using tension monitoring system. This method requires tension monitors installed between dead-end insulators and line structure. One advantage of using this method is that the measured conductor tension can be used in the line strain section employing the ruling span theory. With all due advantages of this system what makes it uneconomic for distribution network is that due to the unbalanced load in different phases, it is possible that the different phases have unequal tension. Therefore, to monitor the tension different devices need to be installed for each phase.

Table 1.1 shows an analysis of various DLR monitoring techniques discussed above. The detailed analysis is available in [15]. From the cost analysis it is clear that all the systems mentioned here are quite expensive and therefore will be infeasible for a distribution network application. Therefore, the system which has been chosen for this purpose in the thesis is GPS monitoring system. This is a comparatively cheaper option and has been successfully tested on a distribution line [16]. This method has been highlighted in green in Table 1.1. A detailed explanation of this method is provided in Section 4.3.

So, to conclude this study of various methods it can be said that distribution systems have a distinct nature from transmission system. The loads are unequally distributed between phases; distribution feeders have unbalanced geometry and are not transposed. The DLR techniques mentioned here were found unsuitable for a distribution system for the reasons mentioned.

Therefore, the algorithm developed in this thesis makes use of the IEEE 738 standard [8] and the State Change Equation to estimate the DLR for a distribution network.

Table 1.1 Different DLR techniques and cost analysis

Method	Brief Introduction	Pros	Cons	Cost
Power Donut	A temperature dependent system first developed in 1988 has over 1000 installations.	-Powered directly from measured conductor -Mature device, has been in use for many years	-Expensive setup	-Configuration dependent, one location system can cost US\$40,000-\$80000
CAT-1 (Nexans)	Tension dependent system installed by over 100 utilities	Reduced price with wide deployment	Limitations: -Span lengths should not differ greatly with ruling span section -Insulator string should be relatively long. -Structure should be rigid	€ 2500 – 3000 per circuit km
Sagometer (Avistar)	Sag dependent system with over 80 units installed in North America	-High accuracy ($\pm 15\text{mm}$)	-Extreme weather conditions like fog, heavy snow may compromise the measurement	Undisclosed
Ampacimon	Sag dependent system with a smart sensor module directly deployed on overhead line. Analyses conductor vibrations and detects fundamental frequencies of the span.	-No calibration required -Does not require external power source	Limitations: -minimum level of current 80 A makes it unsuitable for distribution networks	€ 40,000 + €10,000 per line for real-time measurements + hosting services extra
GPS device system	Sag measuring system	-Economic option. -Tested for distribution networks	- Measurements need to be filtered	GPS device cost (BT-359): \$ 50

1.4 Objectives

1.4.1 General objectives

The key objective of this Master's thesis is to develop and test an algorithm that can be transformed into a monitoring tool that provides the user a graphical representation of real-time ampacity of overhead lines in a distribution system. LabVIEW environment has been used for development of the tool which is a user friendly graphical user interface (GUI). The developed monitoring tool makes use of real-time data inputs of ambient temperature, wind speed and solar radiation from a weather station whereas, the actual line current measurement which is another essential input is received from a PMU.

Apart from the weather data inputs, the developed tool uses PMU measurements of actual line current. The developed application testing has been conducted in the SmarTS Lab by running a real-time hardware in the loop (HIL) simulation of the IDE4L reference grid [17].

1.4.2 Specific objectives

1. Familiarization with the real-time simulator at SmarTS Lab.
2. Familiarization with LabVIEW and its programming environment.
3. Implementation of real-time rating tools in LabVIEW.
4. Configuration of the SEL relay for PMU usage.
5. Test of the monitoring tool in real-time.

1.5 Organization of thesis chapters and description

The thesis report is organized as follows:

In chapter 2, the literature review and algorithm developed for this thesis is presented. A brief introduction to different DLR techniques which were familiarized as literature review is provided, which forms the basis of algorithm developed. The algorithm and its different part including the inputs required for algorithm execution are presented.

In Chapter 3, IEEE 738-2006 [8] standard is discussed. This method is widely used in the development of this thesis. Also, the usage of this standard in the thesis work is explained.

'State Change Equation' is discussed in Chapter 4. The basics of this equation and its usage in the algorithm are presented. Sag measurement technique is also presented in this section.

A form of Kalman filter is used in this thesis to filter out the measurements. This usage and the basics of Kalman filter are presented in Chapter 5.

Chapter 6 is detailed description of the experimental work flow followed in SmarTS lab to conduct testing of the developed algorithm. Various devices and software applications used in testing the application are presented and explained in this section.

The model used for the purpose of testing, the developed LabVIEW application and the results are discussed in Chapter 7.

Chapter 8 presents the conclusion to the entire thesis work. Future work and potential continuation to the application are also discussed in this chapter.

Chapter 2

2 Literature Review and theory development

In this section, the literature review performed for learning the basics of thesis subject as well as the literature crucial for theory development is explained.

2.1 Problem definition

The problem of focus during the course of this thesis is to determine maximum allowable current that can be passed through a distribution line at a given point of time based on actual weather conditions at the physical location of line and actual line loading such that the conductor temperature at no point of time exceeds the maximum specified temperature for the conductor. Mathematically this problem can be stated as [1]:

$$\forall_1 I_{1,t} = \min(I_{1,j,t}) \quad (2.1)$$

$$I_{1,j,t} = f(Ws_{k,j,t}, Wd_{k,j,t}, Ta_{k,j,t}, Sr_{k,j,t}, Tc_{1,j}, C_{1,j}, D_{1,j}) \quad (2.2)$$

$$Tc_{1,j} \leq Tmax_{1,j} \quad (2.3)$$

Where,

I	=	Ampacity
Ws	=	Wind speed
Wd	=	Wind direction
Ta	=	Ambient temperature
Sr	=	Solar radiation
Tc	=	Conductor temperature
C	=	Conductor
D	=	Direction of line
1	=	1, 2, 3.... L transmission lines
j	=	1, 2, 3.... J line sections
t	=	1, 2, 3.... T time
k	=	1, 2, 3.... k weather stations

2.2 Static ratings

Current carrying capability of a transmission line is regarded as constant by power companies; similar is the case with distribution lines. These ratings depend on location of the line and the conductor type. Typical values of ambient temperature, wind speed, solar radiation and maximum conductor temperature used by electrical utilities according to [1] are:

- Ambient temperature = 40°C
- Wind speed = 0.61 m/s
- Solar radiation = 1000 W/m²
- Maximum conductor temperature = 80°C

These figures are conservative values which is not the case in practice as these figures are bounds to change in time. **Appendix A** shows plots of ambient temperature, wind speed and solar radiation for different months (January 2015 – August 2015). These plots give an overview of how values of these quantities change in time.

DLR systems make use of this change in weather conditions to give an ampacity estimate based on the actual conditions. During the time when the values of weather conditions are favorable i.e. less than the conservative estimates, the line can be loaded more without exceeding the maximum allowed conductor temperature. Due to these reasons many power companies are making use of DLR and providing increased line loading capabilities for short durations by considering heat-storage capacity of the conductors [1].

There are numerous methods of DLR estimation. In the following sections some of these techniques are discussed.

2.3 Dynamic line rating techniques

As explained in the previous sections, DLR offers an alternative for network reinforcement. It gives the network opportunity to accommodate the increasing load demand [18]. This section discusses some of the available DLR techniques [1].

2.3.1 Weather dependent systems

These systems are based upon weather parameters. To get efficient line ratings from a weather dependent system, it is important to have real-time access to weather station in vicinity to the line of interest. This weather station should be equipped with an anemometer, wind direction sensor, solar radiation sensor and temperature sensor as explained in [19].

The algorithm developed for line ampacity calculation in this thesis makes use of two different approaches for conductor temperature calculation. These are IEEE 738 standard [8] for calculating current-temperature relationship of bare overhead conductors and the State Change Equation, namely. In order to implement these approaches in real-time, it is very important to have weather data availability in real-time. For this purpose the data is taken directly from a weather station and it provides measurements of the ambient temperature, wind speed and wind direction.

2.3.2 Temperature dependent systems

The temperature dependent systems work on direct measurement of the conductor temperature, for this purpose a device needs to be installed that can determine the conductor temperature in real-time. A study conducted for evaluation of one such device called ‘Power Donut’ has been reported in [12]. This device accurately measures the line current, conductor temperature and ambient temperature. The installed system for this device consists of sensors mounted directly on the conductor of interest or a station bus. Figure 2.1 shows one such installed power donut on an actual line.



Figure 2.1 Power Donut

The study in [20] has introduced one such system developed for rating electric power transmission lines and equipment. The system identifies the conductor span having the lowest ampacity which is then used to determine the ampacity of the entire line. The thermal state of a span is monitored on the measured values of conductor temperature, line current, solar radiation, ambient temperature, and wind speed and wind direction.

In this method, the ampacity of line calculated using the heat balance equation expressed as (2.4), [1].

$$I = \sqrt{\frac{P_r + P_c - P_s}{R_{ac}}} \quad (2.4)$$

Where,

- I = Ampacity
- Pr = Radiation heat loss
- Pc = Convection heat loss due to cooling effect of wind
- Ps = Heat gained by solar radiation
- R_{ac} = Ac resistance of conductor

2.3.3 Tension monitoring systems

Tension monitoring system is yet another technique to determine ampacity of a line, making use of measurements of conductor tension along the line. These systems are based on the fact that conductor tension is a function of conductor temperature. Figure 2.2 [21], shows one such system. The equation relating the conductor stress to conductor temperature is given as in (2.5) [1].

$$\frac{\sigma_2}{E} - \frac{(\omega \cdot L)^2}{24\sigma_2^2} + \alpha(Tc_2 - Tc_1) + \Delta Ec = \frac{\sigma_1}{E} - \frac{(\omega \cdot L)^2}{24\sigma_1^2} \quad (2.5)$$

Where,

- σ_1, σ_2 = Stress at state 1 and state 2 respectively, kg/mm²

- T_{c1}, T_{c2} = Conductor temperature at state 1 and state 2 respectively, $^{\circ}\text{C}$
 E = Young's modulus of elasticity, kg/mm^2
 ω = Specific weight of conductor, $\text{kg}/\text{m}/\text{mm}^2$
 L = Span length, m
 ΔE_c = Inelastic elongation, mm/mm
 α = Coefficient of linear expansion of conductor, $^{\circ}\text{C}^{-1}$

This is general form of the 'State Change Equation' which is later used in the algorithm of line ampacity determination. This method is especially useful in ice-load conditions as the effect of ice and wind loading can be conveniently considered. One disadvantage of this monitoring system is that during the time of installation and maintenance the line has to be taken out of service [1].



Figure 2.2 Tension monitoring system

2.3.4 Sag dependent systems

These systems make use of different techniques to measure the sag of conductor in real-time. As discussed in [18], these systems are generally based on laser or radar scanning. Studies in [22] and [23] introduce some methods of sag monitoring of an overhead line. These systems are usually equipped with an alarming system which helps maintain the clearance level of sag which should at no time exceed the permissible limit. Figure 2.3 [1], shows one such sag monitoring system.

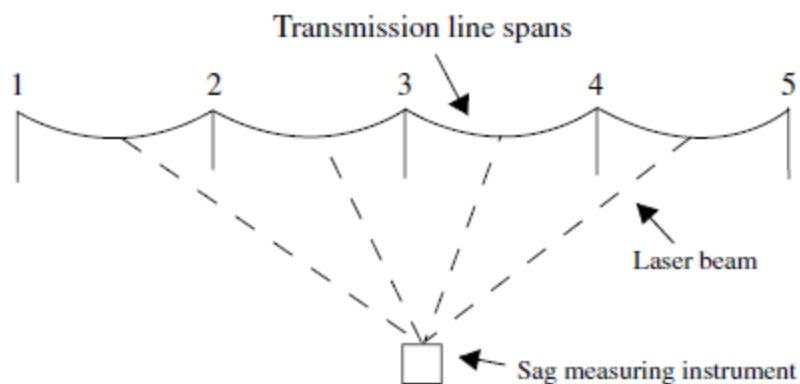


Figure 2.3 Sag-monitoring system

This is an offline monitoring system as it does not require installation of any device on the line [1]. The sag here is measured using a laser beam and

thereby detecting the lowest point of the conductor. Having known the value of conductor sag and with the knowledge of ambient weather conditions it is possible to calculate the real-time ampacity. The equation which relates the conductor sag to conductor tension is given as in (2.6) [1].

$$D = \frac{WL^2}{8T} \quad (2.6)$$

Where,

W = Conductor weight, kg/m
T = Conductor tension, kg

2.3.5 Distributed temperature sensing

Distributed temperature sensing (DTS) is a system which uses sensors to measure temperature by the means of optical fibers. These devices are capable of providing continuous profile of temperature distribution along the cable. The principle of such measurements is mainly based on detecting the backscattering of light.

In [24] there is a review of DTS technology, according to which these systems are highly accurate over significant distances. The accuracy can be as high as $\pm 1^\circ\text{C}$ at a resolution of 0.01°C , over measurements ranging up to 30 km.

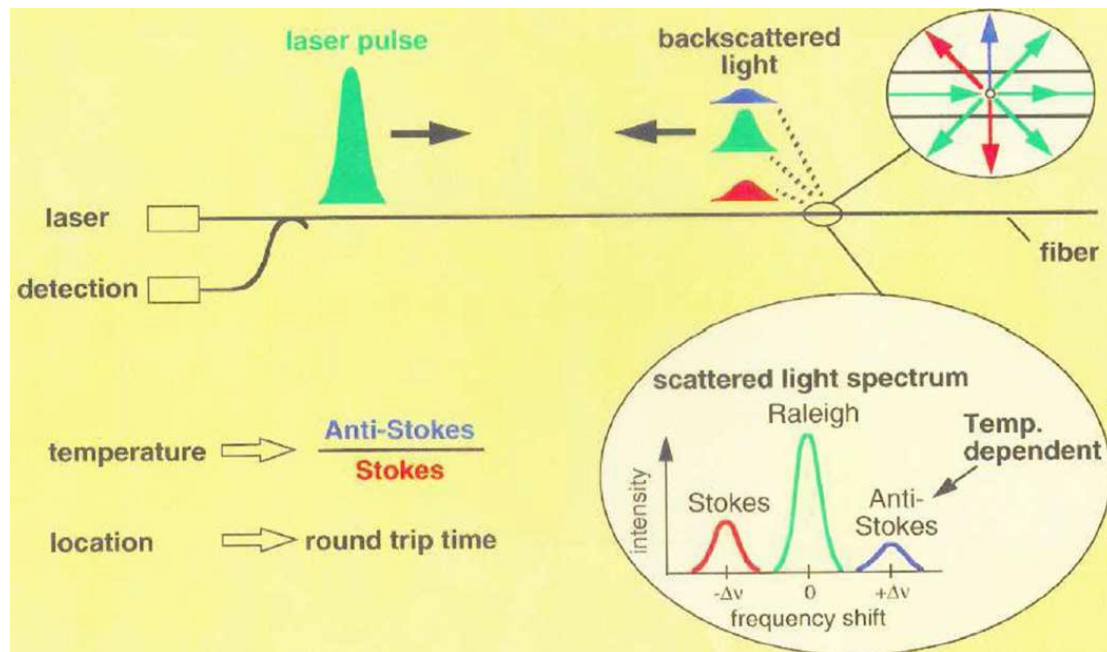


Figure 2.4 DTS using Raman scattering

Figure 2.4 [24], shows the use of DTS technology using Raman scattering which is the inelastic scattering of photon. Here, the local temperature measurement is provided by ratio of Anti-Stokes and Stokes light [25].

2.3.6 Object oriented power line ampacity system

A power line ampacity system which uses object oriented modeling and expert rules of power line environment is presented in [26]. In this system the

ampacity of the conductor is estimated using the solution of conductor temperature differential equations making use of synthetic generation of meteorological data which is adjusted a weather forecast service. This system can be used to get hourly values of powerline ampacity up to seven days in advance.

2.4 Algorithm for real-time dynamic feeder rating

In the previous section various systems for real-time ampacity calculation for an overhead conductor were discussed. All these methods are focused on DLR for transmission networks. In Section 1.3 a detailed review of such methods which have their focus on DLR estimation for transmission network is given. In this thesis work an algorithm has been developed which is focused mainly on distribution network. For this purpose some of the above mentioned methods formed the foundation for the algorithm developed of this thesis. This section introduces the algorithm developed for this thesis. Also brief explanation on importance of various block involved in this algorithm are discussed. In the later sections, a detailed explanation of these blocks is provided.

The method introduced for real time ampacity calculation in this section relies upon real time inputs of line sag, ambient weather condition and line loading. Figure 2.5 shows a block diagram of the developed algorithm for real-time ampacity estimation. The diagram depicts various blocks involved in the algorithm. It can also be seen that data is acquired from different sources at different sampling rates. This is the main reason behind the use of Kalman filter in this algorithm.

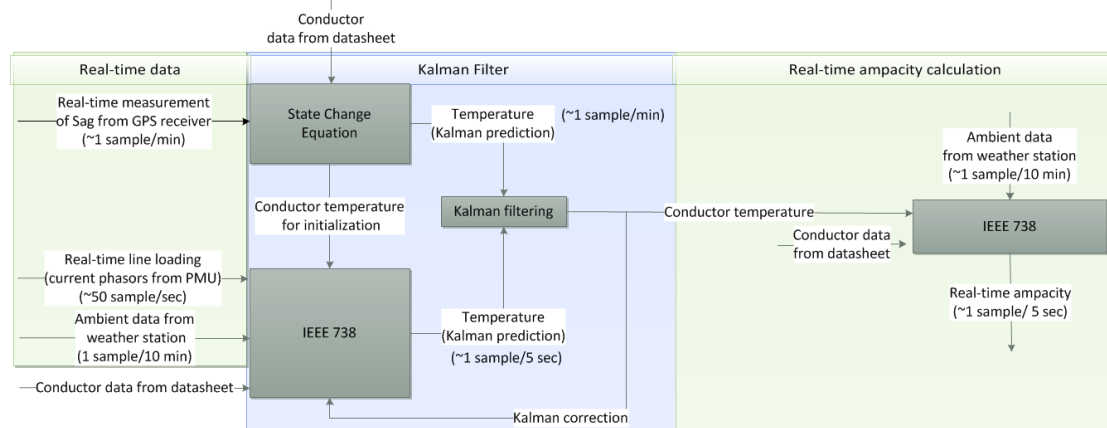


Figure 2.5 Block diagram of real-time ampacity estimation algorithm

In order to successfully implement the algorithm different inputs are required. Table 2.1 is a list of all these inputs and their sources. It should be noted that in this list all the required data is fetched in real-time except for the conductor data which includes conductor weight, diameter, etc. This data unlike the sag measurement, line loading and weather data is fixed and is not subjected to any significant change in time. The sources of these measurement are further explained in the further sections.

Table 2.1 Inputs required for the method and their source

Inputs required	Source	Remark
Real-time sag measurement	GPS device	Measurements from the GPS are bound to have some error. Hence, the conductor temperature calculated is filtered.
Conductor constants	Data sheet	These constants can be known with reasonable accuracy and are not subjected to any significant change in time.
Real-time line loading	Phasor measurement unit	Steady state component of the PMU data is extracted by the Kalman filter
Ambient temperature	Weather station	Weather data from stations located nearest to the lines
Wind velocity and direction	Weather station	
Solar radiation	Weather station	

Once all the data listed in Table 1 is available, the algorithm can be initiated. The block ‘State Change equation’ in Figure 2.5 represents an equation for a conductor which relates one state of the conductor to another state. This means that with the knowledge of parameters of conductor in one state, it is possible to calculate the same parameters in another state. A ‘State’ in this particular reference means the different temperature, stress and load conditions (Detailed explanation is provided in further Chapter 4). When sag measurement and length of ruling span sag is known, the state change equation can be used to calculate the conductor temperature.

‘IEEE738’ is another block in the algorithm based on [8] which is a standard for calculating the current-temperature of bare overhead conductors. A detailed explanation of this standard is given in Chapter 3. There are two ways in which this standard can be used. Firstly when the conductor temperature is known, this standard can be used to calculate the current which caused the known temperature in the conductor. And secondly, when the current through the conductor is known, it can be used to calculate the conductor temperature. In Figure 2.5, the first ‘IEEE738’ block on the left represents the usage of [8] for conductor temperature calculation. Now, with the given inputs of conductor constants, line loading (from PMU) and weather conditions (from online weather station), [8] is used to calculate conductor temperature.

It should be noted that in order to use the blocks discussed here it is very important that initial conditions are known. This means that a known state for the state change equation and initial conductor temperature for the ‘IEEE738’ block.

Kalman filter which can be briefly defined as an algorithm which produces estimates of variable which are more precise than the input noise laden variables given to it. It reduces the inaccuracies and provides a better estimate. The Kalman filter is explained in detailed in Chapter 5. Now that the conductor temperature has been calculated using two different methods, a Kalman filter is used to refine these measurements and give a more accurate conductor temperature estimate.

With accurate estimation of the conductor temperature, the standard in [8] is brought to use again, this time to calculate ampacity of the conductor. Apart from the measured conductor temperature, other inputs required here are the conductor constants, real-time weather conditions and actual line loading. The real-time line loading, required in this application is the steady state component of the PMU data. The final Real-time ampacity can be seen in a graphical form in the application developed in LabVIEW environment.

Chapter 3

3 IEEE 738 standard for calculating the current-temperature of bare overhead conductors

IEEE 738 [8] is a standard method for calculating the current-temperature of bare overhead lines. This standard has been successfully implemented in various real-time ampacity calculations applications. The ratings can be calculated in real-time given that the following quantities are known [8]:

- Conductor material properties and conductor diameter
- Conductor surface conditions
- Ambient weather conditions
- Conductor electrical current

Conductor material properties, diameter and surface conditions are specific chemical and physical properties that are not subjected to any significant change in short time span. These quantities differ for every conductor which makes it essential to update them according to the conductor for which the calculations have to be conducted. **Appendix B** contains datasheet of the conductor that has been used to test this application.

The conductor surface conditions on the other hand may vary in time depending upon the surroundings and ambient atmospheric conditions, as an example the wind speed and ice loading can have a significant impact on the conductor surface conditions.

In order to perform accurate calculations it is important to have reliable ambient weather conditions. Weather conditions like wind speed, wind direction, ambient temperature and solar radiations are some of the most important inputs required while using the standard [8] as they have a major impact on the conductor temperature and thereby on the ampacity estimate. To get an idea on how much these quantities can vary in time, **Appendix A** can be referred which contains the plots of ambient temperature, wind speed and solar radiation for different months (January 2015 – August 2015).

Conductor electrical current can either be a constant or a time varying quantity depending on the power system loading, generation dispatch, faults, etc. In this thesis as the model used is executed in an HIL setup, the line loading is received in real-time from a PMU installed in SmarTS lab. Further explanation on this setup is given in Chapter 6.

3.1 Term definitions

Definitions of some parameters and assumptions related to them are enlisted in this section. All these definitions are given by [8].

3.1.1 Conductor temperature

The conductor temperature is assumed to be isothermal that is the heat transfer into or out of the system happens at a slow rate such that the thermal

equilibrium is maintained. In the context of the conductor it would mean that there are no axial or radial temperature variations. This stands true for all steady-state calculations as well as for transient calculations where time period of interest exceeds 1 minute or the conductor consists of a single material.

3.1.2 Heat capacity

The heat capacity (dQ_c/dT_c) is the ratio of quantity of the heat added (dQ_c) and the temperature increment (dT_c) which is result of the former addition of heat.

3.1.3 Reynolds number

Is a non-dimensional quantity which is equal to the product of air velocity (V_w) and the conductor diameter divided by the kinematic viscosity (μ_f/ρ_f).

3.1.4 Specific heat

The specific heat of a conductor is its heat capacity divided by its mass.

3.2 Calculations

Using [8] it is possible to calculate thermal rating of a conductor in different conditions. These calculations are specific to whether the line is being operated in a steady-state, a transient state, fault state and time-varying weather and current state. In this section the different conditions are briefly discussed.

3.2.1 Steady state calculations

Steady state refers to a condition of thermal equilibrium. Thermal rating of the conductor in steady state is the maximum constant current which considering the ambient conditions and conductor constants yield the maximum allowable temperature specified for the conductor.

Whereas calculation of steady state conductor temperature is an iterative process as radiation and convection heat loss rates (detailed description in section 3.4) are not linearly dependent. The process starts with making an assumption for the conductor temperature which is then used to calculate the heat losses. Equation (3.4) can then be used to calculate the conductor current that has resulted in this temperature. This current is then compared to the given conductor current and is then modified until the calculated current equals the given current.

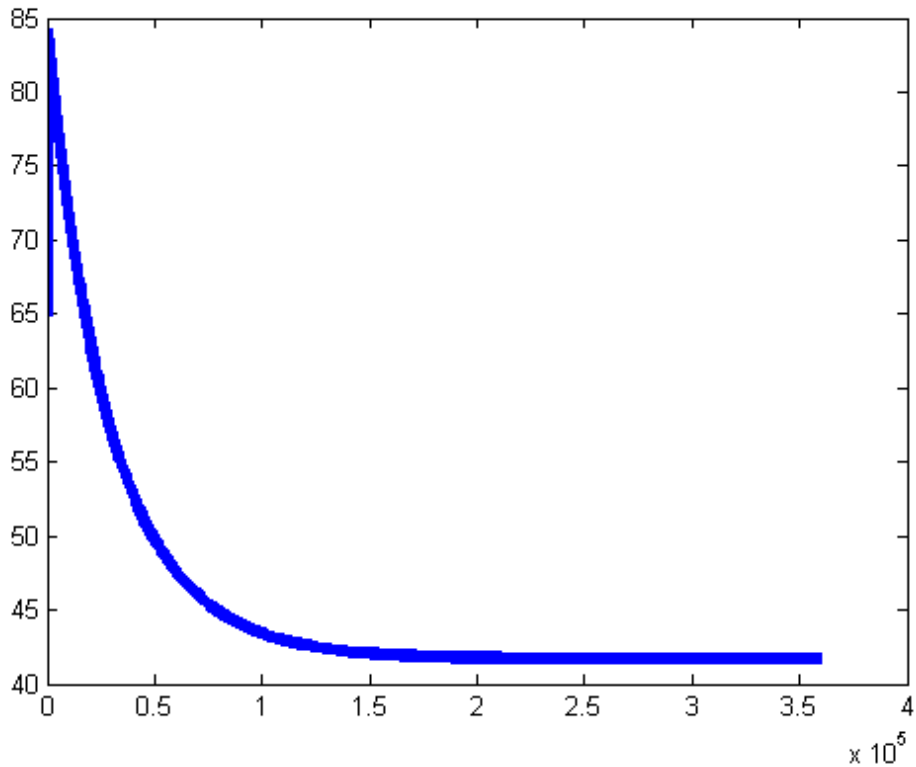


Figure 3.1 Steady state conductor temperature

The steady state conductor temperature calculation algorithm was implemented in MATLAB. Figure 3.1 show the convergence of the conductor temperature in a steady state.

3.2.2 Transient calculations

Transient calculation differ from steady state calculations in that, in transient case the thermal rating is the final current that results in maximum allowable conductor temperature in a specified time after a step change in the line loading.

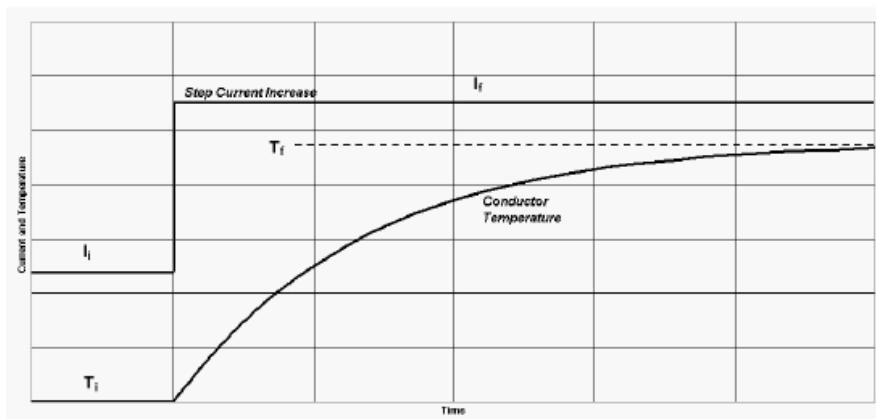


Figure 3.2 Step change

Figure 3.2 [8], demonstrates the corresponding effect of step change in current on the conductor temperature.

In order to calculate transient thermal rating of the conductor, the conductor temperature is calculated over a range of current values. The current value that causes the maximum conductor temperature becomes the transient thermal rating.

3.2.3 Time-varying weather and current calculations

Real-time ratings of a conductor which take into account the changing weather and current can be calculated by using the method provided by [27]. The calculation methods explained earlier can be used for this purpose. A series of calculations is done each of which applies to a short interval of time, during this period the conductor current and ambient conditions are assumed to be constant and equivalent to the values at the beginning of the interval.

3.3 Symbols and Description

The standard in [8] consists of numerous equations which are expressed different symbols. Table 3.1 is a list of all these symbols, their short description and SI units.

Table 3.1: Symbol, Description and SI units

Symbol	Description	SI units
A'	Projected area of conductor per unit length	m^2/m
C	Solar azimuth constant	Degrees
C_{pi}	Specific heat of conductor i^{th} material	$J/(kg \cdot ^\circ C)$
D	Conductor diameter	mm
H_c	Altitude of sun	degrees
H_e	Elevation of conductor above sea level	m
I	Conductor current	A
I_i	Initial current before step change	A
I_f	Final current after step change	A
K_{angle}	Wind direction factor	-
K_{solar}	Solar altitude correction factor	-
k_f	Thermal conductivity of air at temperature T_{film}	$W/(m \cdot ^\circ C)$
Lat	Degrees of latitude	degrees
mC_p	Total heat capacity of conductor	$J/(m \cdot ^\circ C)$
m_i	Mass per unit length of i^{th} conductor material	Kg/m
N	Day of the year	-
P_{loss}	Ohmic loss	W/m
$q_{cn}, q_{c1}, q_{c2}, q_c$	Convected heat loss rate per unit length	W/m

q_r	Radiated heat loss rate per unit length	W/m
q_s	Heat gain rate from sun	W/m
Q_s	Total solar and radiated heat flux rate	W/m ²
Q_{se}	Total solar and sky radiated heat flux rate elevation corrected	W/m ²
$R(T_c)$	AC resistance of conductor at temperature, T_c	Ω/m
T_a	Ambient air temperature	$^{\circ}C$
T_c	Conductor temperature	$^{\circ}C$
T_{film}	$(T_c + T_a)/2$	$^{\circ}C$
T_{low}	Minimum conductor temperature for which ac resistance is specified	$^{\circ}C$
T_{high}	Maximum conductor temperature for which ac resistance is specified	$^{\circ}C$
V_w	Speed of air stream at conductor	m/s
Z_c	Azimuth of sun	Degrees
Z_l	Azimuth of line	degrees
Δt	Time step used in transient calculation	s
ΔT_c	Conductor temperature increment corresponding to time step	$^{\circ}C$
α	Solar absorptivity (0.23 to 0.91)	-
δ	Solar declination (0 to 90)	degrees
ϵ	Emissivity (0.23 to 0.91)	-
τ	Thermal time constant of the conductor	s
Φ	Angle between wind and axis of conductor	degrees
β	Angle between wind and perpendicular to conductor axis	Degrees
ρ_f	Density of air	kg/m ³
θ	Effective angle of incidence of the sun's rays	Degrees
μ_f	Dynamic viscosity of air	Pa-s
ω	Hours from local sun noon times 15	Degrees
χ	Solar azimuth variable	-

3.4 Formulas

In the following section various formulas used to implement the standard [8] and develop this thesis algorithm are given.

3.4.1 Steady state heat balance

As per the law of conservation of energy, the rate of heat loss and rate of heat gain are always in balance. In the context of conductor this balance is given by (3.1) and (3.2) [8].

$$Heat_{gain} = Heat_{loss} \quad (3.1)$$

$$q_c + q_r = q_s + P_{loss} \quad (3.2)$$

where,

$$P_{loss} = I^2 R(T_c) \quad (3.3)$$

P_{loss} here represents the ohmic loss which causes a heat gain in the conductor. Equation (3.4) [8], which is a modulation of heat balance equation is used for ampacity calculation.

$$I = \sqrt{\frac{q_c + q_r - q_s}{R(T_c)}} \quad (3.4)$$

3.4.2 Non-steady state heat balance

Equations (3.5) and (3.6) [8], represent the non-steady state heat balance equation for the conductor.

$$q_c + q_r + mC_p \frac{dT_c}{dt} = q_s + I^2 R(T_c) \quad (3.5)$$

$$\frac{dT_c}{dt} = \frac{1}{mC_p} [R(T_c)I^2 + q_s - q_c - q_r] \quad (3.6)$$

3.4.3 Convection heat loss rate

Equations (3.7) and (3.8) [8], are used to calculate forced convection heat loss rate (q_c). Equation (3.7) is used for convection heat loss rate calculation when the wind speed is low; this equation is invalid for high wind speeds. On the other hand equation (3.8) [8] is applicable at high wind speeds.

$$q_{c1} = \left[1.01 + 0.0372 \left(\frac{D\rho_f V_w}{\mu_f} \right)^{0.6} k_f K_{angle} (T_c - T_a) \right] \quad (3.7)$$

$$q_{cz} = \left[0.0119 \left(\frac{D\rho_f V_w}{\mu_f} \right)^{0.6} k_f K_{angle} (T_c - T_a) \right] \quad (3.8)$$

As mentioned in the Table 3.1 K_{angle} is the wind direction factor; this factor is multiplied by the convective heat loss rate. Equation (3.9) [8], is used to calculate the wind factor. Here, ϕ is the angle between the wind direction and the conductor axis.

$$K_{angle} = 1.194 - \cos(\phi) + 0.194 \cos(2\phi) + 0.368 \sin(2\phi) \quad (3.9)$$

The wind direction factor can also be calculated as a function of β which is the angle between the wind direction and a perpendicular to the conductor axis. The expression is shown in equation (3.10) [8].

$$K_{angle} = 1.194 - \sin(\beta) - 0.194 \cos(2\beta) + 0.368 \sin(2\beta) \quad (3.10)$$

3.4.4 Natural convection

When the wind speed at location of the conductor is zero, natural convection occurs. In this case the convection heat loss is given as (3.11) [8].

$$q_{cn} = 0.0205 \rho_f^{0.5} D^{0.75} (T_c - T_a)^{1.25} \quad (3.11)$$

According to [8], it is recommended that larger of forced and natural convection heat losses should be used at low wind speeds.

$$T_{film} = \frac{T_c + T_a}{2} \quad (3.12)$$

3.4.5 Radiated heat loss rate

Equation (3.13) [8], gives the expression for calculation of radiated heat loss.

$$q_r = 0.0178 D \varepsilon \left[\left(\frac{T_c + 273}{100} \right)^4 - \left(\frac{T_a + 273}{100} \right)^4 \right] \quad (3.13)$$

3.4.6 Rate of solar heat gain

Equation (3.14) [8], give the expression for calculation of rate of solar heat gain.

$$q_s = \alpha Q_{se} \sin(\theta) A' \quad (3.14)$$

where,

$$\theta = \arccos[\cos(H_c) \cos(Z_c - Z_l)] \quad (3.15)$$

3.4.7 Conductor electrical resistance

Equation (3.16) [8], is used to calculate electrical resistance of the conductor at a specific temperature.

$$R(T_c) = \left[\frac{R(T_{high}) - R(T_{low})}{T_{high} - T_{low}} \right] (T_c - T_{low}) + R(T_{low}) \quad (3.16)$$

3.4.7.1 Skin effect

The conductor resistance given in dc has to be converted to dc resistance. The conductor dc resistance is given according to [28] as:

$$R_{dc} = R_{20}(1 + \alpha(T - 20)) \quad (3.17)$$

Where,

- R_{dc} = Conductor dc resistance at temperature T, Ω
- R_{20} = Conductor temperature at 20 $^{\circ}\text{C}$, Ω
- T = Operating temperature of conductor, $^{\circ}\text{C}$
- α = Temperature coefficient of resistance, $1/^{\circ}\text{K}$

When the dc resistance of the conductor is known, it is possible to calculate the conductor ac resistance also taking into account the skin effect factor and proximity effect factor. Although as in the course of this thesis only overhead lines are considered, the proximity effect factor is equivalent to zero. The expression for conductor ac resistance is given as:

$$R_{ac} = R_{dc}(1 + y_s + y_p) \quad (3.18)$$

Where,

- y_s = Skin effect factor
- y_p = Proximity effect factor (zero for overhead lines)

The skin effect factor for a conductor is calculated using the following expression:

$$y_s = \frac{x_s^4}{192 + 0.8 * x_s^4} \quad (3.19)$$

Where,

- x_s = $\sqrt{\frac{8\pi f}{R_{dc}} * 10^{-7} * k_s}$
- f = Supply frequency, Hz
- k_s = Skin effect coefficient (1 for bare conductors)

3.4.8 Equations for air properties, solar angles and solar flux

The standard [8] gives an expression (3.20) that is formed using least square polynomial regression method on data of thermal conductivity, total heat flux

and solar heat correction for elevation. The algebraic equations for these are given in the following section.

$$Y = A + BX + CX^2 + DX^3 + EX^4 + FX^5 + GX^6 \quad (3.20)$$

3.4.8.1 Dynamic viscosity of air

$$\mu_f = \frac{1.458 \times 10^{-6} (T_{film} + 273)^{1.5}}{T_{film} + 383.4} \quad (3.21)$$

3.4.8.2 Air density

$$\rho_f = \frac{1.293 - 1.525 \times 10^{-4} H_e + 6.379 \times 10^{-9} H_e^2}{1 + 0.00367 T_{film}} \quad (3.22)$$

3.4.8.3 Thermal conductivity of air

$$k_f = 2.424 \times 10^{-2} + 7.477 \times 10^{-5} T_{film} - 4.407 \times 10^{-9} T_{film}^2 \quad (3.23)$$

3.4.9 Altitude of the sun

Equation (3.24) [8], is used to calculate solar altitude of sun. The equations hold validity for all latitudinal locations.

$$H_c = \arcsin[\cos(Lat) \cos(\delta) \cos(\omega) + \sin(Lat) \sin(\delta)] \quad (3.24)$$

Where δ (solar declination) is calculated using the following expression,

$$\delta = 23.4583 \sin \left[\frac{284 + N}{365} 360 \right] \quad (3.25)$$

3.4.10 Azimuth of sun

Equation (3.26) [8], is used for calculation of Azimuth of sun which is an angular measurement in a spherical coordinate system.

$$Z_c = C + \arctan(\chi) \quad (3.26)$$

where,

$$\chi = \frac{\sin(\omega)}{\sin(Lat) \cos(\omega) - \cos(Lat) \tan(\delta)} \quad (3.27)$$

Table 3.2 [8], gives the solar azimuth constant for different hour angles (ω) and azimuth variable (χ).

Table 3.2: Solar azimuth constant

“Hour Angle,” ω (degrees)	C if $\chi \geq 0$ (degrees)	C if $\chi < 0$ (degrees)
$-180 \leq \omega < 0$	0	180
$0 \leq \omega \leq 180$	180	360

3.4.11 Total heat flux received by a surface at sea level

Equation (3.30) [8], is used to calculate total heat flux. The solar heat flux density is directly dependent on the atmospheric conditions. Table 3.3 [8], gives the values of coefficients used in the equation for a clear atmosphere and industrial atmosphere.

$$Y = \text{total heat flux, } Q_s (\text{w/m}^2) \quad (3.28)$$

$$X = \text{solar altitude, } H_c (\text{degrees}) \quad (3.29)$$

$$Q_s = A + BH_c + CH_c^2 + DH_c^3 + EH_c^4 + FH_c^5 + GH_c^6 \quad (3.30)$$

Table 3.3: Coefficient values in clear and industrial atmosphere

Coefficients	Clear atmosphere	Industrial atmosphere
A	-42.2391	53.1821
B	63.8044	14.2110
C	-1.9220	6.6138×10^{-1}
D	3.46921×10^{-2}	-3.1658×10^{-2}
E	-3.61118×10^{-4}	5.4654×10^{-4}
F	1.94318×10^{-6}	-4.3446×10^{-6}
G	-4.07608×10^{-9}	1.3236×10^{-8}

3.4.12 Total heat flux elevation correction factor

Equation (3.31) [8], is used to calculate total heat flux elevation correction factor.

$$Q_{se} = K_{solar} Q_s \quad (3.31)$$

Where,

$$K_{solar} = A + BH_e + CH_e^2 \quad (3.32)$$

$$A = 1$$

$$B = 1.148 \times 10^{-4}$$

$$C = -1.108 \times 10^{-8}$$

3.5 Use of the standard in algorithm

For the purpose of this thesis, IEEE standard given in [8] is used two times in the algorithm, the explanation for which is given in the following sections.

3.5.1 To calculate conductor temperature

Convection heat and radiation loss rates are not linearly dependent on the conductor temperature. For this reason conductor temperature is calculated in terms of the real time current and weather conditions. The process is as follows [8]:

- A conductor temperature is assumed.
- For this temperature corresponding heat losses are calculated.
- The conductor current that yields this temperature is calculated
- The calculated current is compared to the given conductor current.
- The conductor temperature is then increased or decreased until the calculated current equals the given current

3.5.2 Ampacity calculation

For a conductor with the known values of conductor temperature and weather parameters like wind speed, ambient temperature, solar radiation, etc. in real time, the heat losses due to convection and radiation, solar heat gain and conductor resistance can be calculated. These calculated terms can then be used to calculate the corresponding conductor temperature [8].

Chapter 4

4 State change equation

The application developed in this thesis work relies on real-time sag measurements to calculate the conductor temperature. Hence, it is important to have an expression which defines the relationship between the conductor span sag and conductor temperature. State change equation which is also known as condition change equation is an equation which relates two states of an overhead line such that if parameters for one state are known, the parameters can be calculated for another state. Here, state refers to different levels of temperature, tension and specific load on the conductor. State change equation has been in existence for a long time and it has been broadly used for mechanical calculation of overhead lines for transmission and distribution of electric power.

The state change equation in its general form is a cubic polynomial function which is solved using numerical and trial-error methods. A method developed for using state change equation for direct calculation which gives accurate results has been introduced in [29]. This method is explained in detail in the following section.

4.1 Formulas

The paper presented in [29] gives an expression for state change equation given as in (4.1).

$$\sigma^3 - \sigma^2 \left(\sigma_0 - \alpha E(t - t_0) - \frac{\alpha^2 g_0^2 E}{24\sigma_0^2} \right) = \frac{\alpha^2 g^2 E}{24} \quad (4.1)$$

The simplified equation can now be written as:

$$\sigma^3 - \sigma^2 A = B \quad (4.2)$$

$$A = \sigma_0 - \alpha E(t - t_0) - \frac{\alpha^2 g_0^2 E}{24\sigma_0^2} \quad (4.3)$$

$$B = \frac{\alpha^2 g^2 E}{24} \quad (4.4)$$

Where,

- α = Linear Thermal Expansion Coefficient, $1/^\circ\text{C}$
- E = Elasticity Modulus, kg/mm^2
- σ_0 = Traction stress in initial conditions, kg/mm^2
- σ = Traction stress in final conditions, kg/mm^2
- t_0 = Temperature in initial conditions, $^\circ\text{C}$
- t = Temperature in final conditions, $^\circ\text{C}$

- g_0 = Specific Load per unit of length in initial conditions, kg/m.mm²
 g = Specific Load per unit of length in final conditions, kg/m.mm²

As discussed earlier, the problem with the state change equation in the general is that it is a third degree polynomial function, which means it has three roots which can be either positive, negative or complex numbers. As a solution to this problem, [29] has developed an algebraic expression that allows solving this equation in a convenient manner.

The two equations which are solved to get the conductor temperature in the new state are [29]:

$$A = \sigma_0 - \alpha E(t - t_0) - \frac{a^2 g_0^2 E}{24\sigma_0^2} \quad (4.5)$$

And

$$\sigma = \sqrt[3]{-\frac{\left(-\frac{2A^3}{27} - B\right)}{2} + \sqrt{\frac{\left(-\frac{2A^3}{27} - B\right)^2}{4} + \frac{\left(-\frac{A^2}{3}\right)^3}{27}}} + \sqrt[3]{-\frac{\left(-\frac{2A^3}{27} - B\right)}{2} - \sqrt{\frac{\left(-\frac{2A^3}{27} - B\right)^2}{4} + \frac{\left(-\frac{A^2}{3}\right)^3}{27}}} + \frac{A}{3} \quad (4.6)$$

Table 4.1 enlists sample data for an ACSR 1/0. These data specifications are directly taken from the conductor data sheet provided in the **Appendix B** of this thesis report.

Table 4.1: ACSR data

ACSR characteristic data	Symbol	Unit	Quantity
Total real cross section area	S	mm ²	62.45
Overall diameter	D _c	mm	10.1
Unit weight of the cable	p _c	kg/m	0.216
Thermal expansion coefficient	α	1/°C	19.3 * 10 ⁻⁶
Elasticity modulus	E	kg/mm ²	76000

Parameters for the conductor are enlisted in Table 4.2. As explained earlier, in order to use the state change equation it is essential to have known parameters for at least one state of the conductor. The basic state here is the known state for which the stress is known at a specific temperature, wind velocity and specific load. Whereas, final state stress has been calculated using the known values of wind velocity and temperature. The specific load on the conductor has to be calculated accurately to get reliable results from the state

change equation. The calculation of specific load is done using the method described in the following section. The final state calculated values are then used for temperature calculation.

Table 4.2: Conductor parameters

Parameters	Unit	Basic state	Final state
Temperature	^o C	t _o = 23	t = 42
Wind velocity	km/h	v _o = 0	v = 2
Specific load	kg/m.mm ²	g _o = 3.46 * 10 ⁻³	g = 0.0035
Stress	Kg/mm ²	σ _o = 3.76	σ = 2.67

4.2 Determination of specific wind load

In order to generate an accurate state change relation for the conductor, it is important to calculate the specific load accurately. The following method is used for the purpose.

Wind load on per unit length of a conductor is calculated using the formula:

$$g = 0.75k \frac{v^2}{16} D_c \left(0.6 + \frac{80}{a}\right) \sin\theta \quad [kg/m] \quad (4.7)$$

In absence of wind the formula used to calculate specific load is:

$$g_0 = \frac{p_c}{S} \quad (4.8)$$

Where,

- v = velocity of wind m/s
- k = dynamic pressure coefficient (Table 4.3)
- D_c = diameter of conductor, m
- a = elevation, m
- θ = Wind direction
- P_c = Conductor weight, kg/m
- S = Span length, m

Table 4.3: Dynamic pressure coefficient

D _c	k
D_c ≤ 12.5	1.2
12.5 < D_c ≤ 15.8	1.1
15.8 < D_c	1.0

It can be seen from (4.7) that the specific weight of the conductor is dependent on the velocity of wind. The algorithm developed in this thesis has real-time measurements of wind velocity which helps to calculate accurate value of specific weight. The precision of this value has a direct impact on the conductor temperature calculation using state change equation.

4.3 Sag measurement method

Current carrying conductors of transmission and distribution lines elongate with time, temperature and tension [7], this variation in the conductor results in line sag. Figure 4.1 shows a sagging overhead line. In an overhead line, the sag can be influenced by many different factors like ambient weather conditions, weight of the conductor, the current passing through conductor and length of the span. Apart from these factors, wind speed and direction and ice loading also has a significant impact on the conductor sag. This means that the sag is always changing and hence a reliable method is necessary for sag measurement.



Figure 4.1 Line sag

There are numerous methods available to measure real-time sag of a transmission line. Unfortunately there are not many methods which focus on distribution lines and as the focus of this thesis is on DLR application for distribution lines, a suitable method was found in [16].

This method is based on measurements received from a GPS device. The real time sag measurements are derived from the measurements provided by the GPS receiver which is strategically placed in the middle of span under inspection. This method has been previously tested for 440V distribution line [16]. Figure 4.2 [16], shows the basic setup used for real time sag measurement.

GPS receivers provide measurements in form of latitude, longitude and its altitude hence it is crucial to have the altitude of conductor above sea level. High precision GPS devices are available which can be used for this purpose.

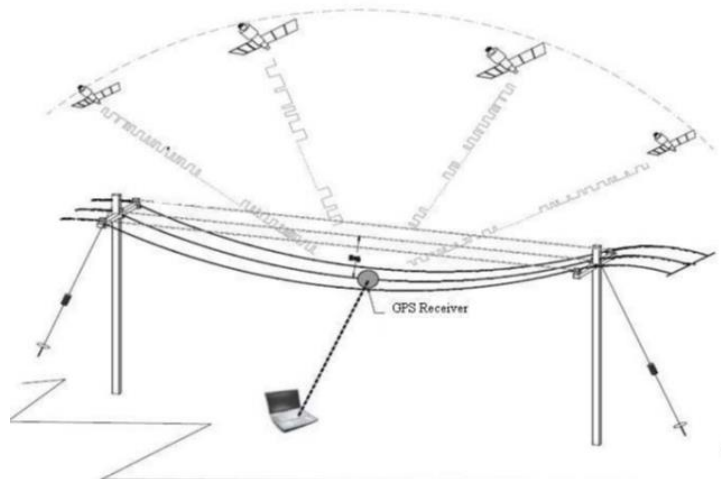


Figure 4.2 GPS device placement

4.3.1 Sag level monitoring

Conductor sag is directly related to the conductor temperature. All conductors have a manufacturer specified maximum allowable temperature limit which at no point in time should be exceeded in order to maintain a safe operation. Increasing value sag, amongst other things is an indication that the conductor temperature is increasing. In the application developed for this thesis, the limits have been specified for maximum sag. The sag level is constantly compared with the maximum allowed sag limit which when exceeded triggers an alarm. Figure 4.3, demonstrates the simple algorithm which can be used by user of this application to maintain the safety limit of both sag and conductor temperature.

This algorithm serves two purposes, firstly the ground clearance of the conductor is always maintained and secondly, as conductor sag is directly related to its temperature (given by state change equation), an alarm would indicate whether or not the permissible temperature limit is exceeded.

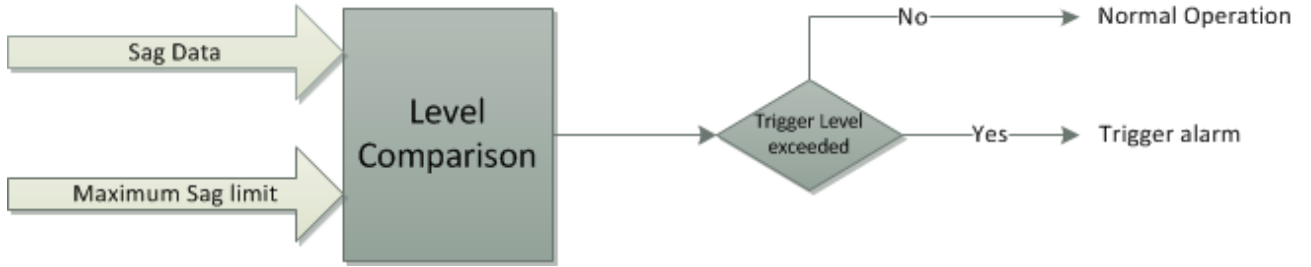


Figure 4.3 Sag alarm triggering algorithm

4.3.2 Ruling span sag

The concept of ruling span has been utilized in this thesis. It is method used to approximate the tension within a multi-span dead-ended section of lines. The method has been analyzed in [29] according to which the ruling span approach can be utilized with little error for an overhead line to predict sags in suspension spans. Ruling span can be defined as [30] ‘A level dead-end span that gives the same change in tension from changes in loading, creep, and/or temperature as that in a series of suspension spans between two dead-ends structures’.

The expression for ruling span is given as [30]:

$$S_r = \sqrt{\frac{\sum S_i^3}{\sum S_i}} \quad (4.9)$$

Where,

- S_r = Ruling span length, m
- S_i = Suspension span length, m

The equation (4.9) is applicable to single level dead-end suspensions. The spans can either be same length or different. The use of ruling span sag is important in this thesis work as the model [17] on which the developed application is tested is based on IEEE-34 bus feeder. And although line length specifications have been provided along with this model but there is no

information about the number of spans between two consecutive buses and their respective lengths. Hence, reasonable assumptions had to be made about these individual span lengths. Table 4.4 shows the line data of IEEE-34 bus feeder model. Details of this model will be discussed in Chapter 6 and 7.

Table 4.4: Line data for IEEE 34-bus feeder

Node A	Node B	Length(ft.)	Configuration
800	802	2580	300
802	806	1730	300
806	808	32230	300
808	810	5804	303
808	812	37500	300
812	814	29730	300
814	850	10	301
816	818	1710	302
816	824	10210	301
818	820	48150	302
820	822	13740	302
824	826	3030	303
824	828	840	301
828	830	20440	301
830	854	520	301
832	858	4900	301
832	888	0	XFM-1
834	860	2020	301
834	842	280	301
836	840	860	301
836	862	280	301
842	844	1350	301
844	846	3640	301
846	848	530	301
850	816	310	301
852	832	10	301
854	856	23330	303
854	852	36830	301
858	864	1620	302
858	834	5830	301
860	836	2680	301
862	838	4860	304
888	890	10560	300

Chapter 5

5 Kalman filter

This thesis focuses on calculating the conductor temperature from two different approaches and then filtering them in order to get a refined and more accurate result. An optimal filter for this approach is a Kalman filter. This section explains the basic Kalman filter and how it is being used in the developed algorithm.

Kalman filter is a filtering technique that uses a series of measurements observed over time. It produces estimates of unknown variables that tend to be more precise than those based on direct measurement. The raw data received from the GPS device consists of error which affects the accuracy of position measurement. The accuracy of the measurements is dependent on a number of factors like the type of measurement made, ionospheric and tropospheric conditions, government inserted error affected as a security measure, number of satellites in view, receiver equipment used, digital signal processing of the received signal, surface features, reflection of signals, and other factors [2]. This will have an impact on the calculated temperature, hence in order to get trustable results the measurements provided by the GPS device need to be processed, which in this method is achieved by the use a Kalman filter.

Kalman filter is basically a set of equations that consist of two main stages namely prediction and correction. The estimator is optimal in the sense that it minimizes the estimated error covariance given that some presumed conditions are met [31]. The equations in Figure 5.1 are the general equations of a Kalman filter. Here the first block on the left contains the prediction of state ahead and error covariance of that state whereas the second block on the right updates the predicted state using the Kalman gain (K).

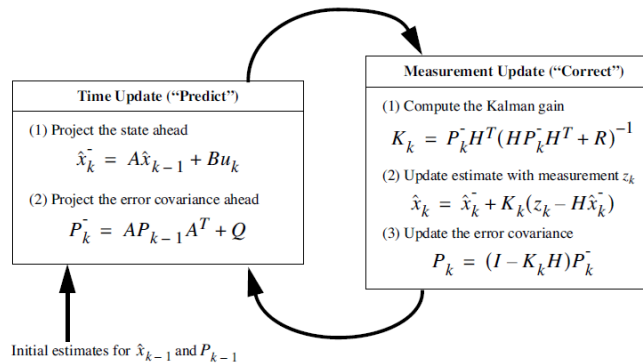


Figure 5.1 Operation of a Kalman filter

- $\mathbf{x}_k \in \mathfrak{R}^s$ and $\mathbf{x}_{k-1} \in \mathfrak{R}^s$ represent the system state at the current time step k and at the previous time step $k-1$, respectively.

- $\mathbf{u}_k \in \mathcal{R}^l$ represents a set of control variables at time step k .
- \mathbf{A} is an $s \times s$ matrix that links the system state at the current time step k with the state at the previous time step $k-1$. Matrix \mathbf{A} might change at each time step.
- \mathbf{B} is an $s \times l$ matrix that relates the system state to the control variables at time step $k-1$.
- $\mathbf{z}_k \in \mathcal{R}^m$ represents the set of measurements at time step k .
- \mathbf{H} is an $m \times s$ matrix that relates the measurements set and the system state, both referred to the current time step k .

In order to ensure the accuracy of Kalman filter performance it is crucial to use correct inputs for measurement (R) and process noise covariance (Q) matrices. R is generally given as the accuracy of the measurement device whereas Q can be updated at every step or it can be made to be a fixed optimal value.

5.1 Implementation and effect of Kalman filter

Figure 5.2 represents the LabVIEW implementation of Kalman filter in the developed algorithm. As explained in the previous section, Kalman filter is a two-step approach, these steps are prediction and correction namely. Once all the required input data to execute the IEEE 738 [8] standard and ‘state change equation is available’, the conductor temperatures are calculated individually from both the methods, this forms the prediction step of Kalman filter. These estimates of conductor temperature are then fed to the Kalman filter. Using the filter a better estimate of conductor temperature is calculated. And as it can be seen in the Figure 5.2, this temperature from the Kalman filter goes back to the IEEE 738 block as a feedback. This forms the correction step of Kalman filter. The process is continued for every step to generate filtered temperature estimate.

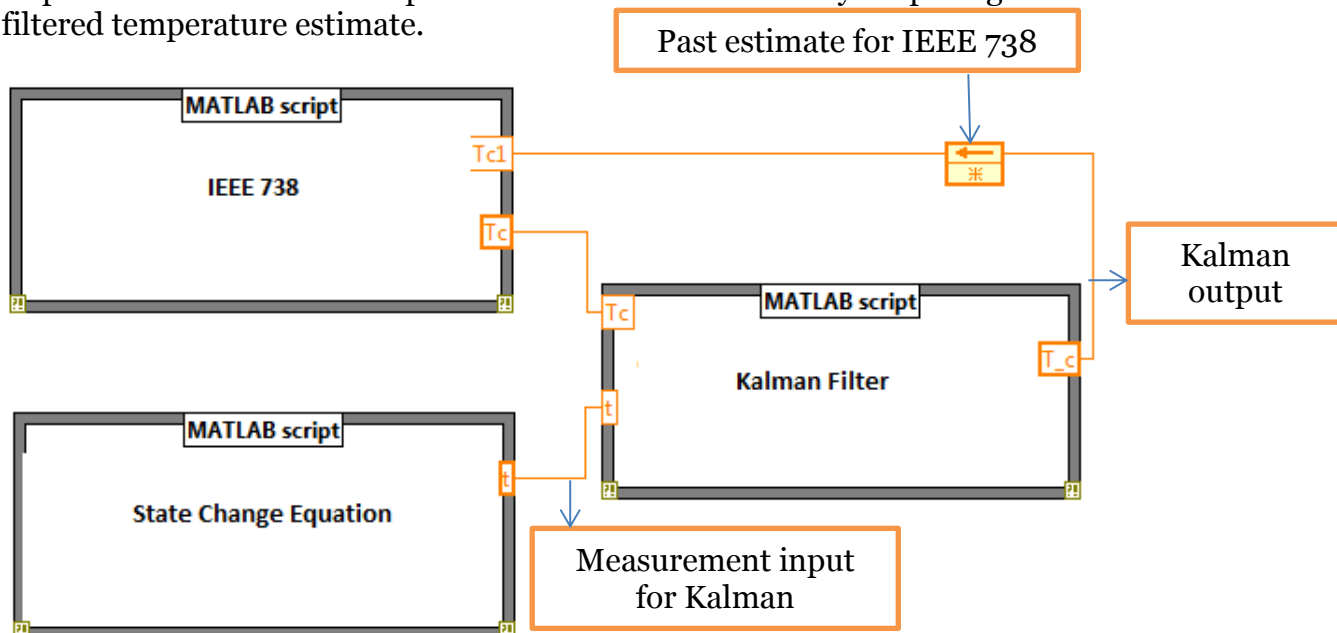


Figure 5.2 Kalman filter implementation

The effect of implementing Kalman filter can be seen in the Figure 5.3. On running the application in LabVIEW, generated results used to plot the conductor temperature. The red and green line in this plot indicates the

temperature calculated using the 'state change equation' and IEEE 738 standard [8] respectively. The blue line indicates the filtered conductor temperature. The operation of Kalman filter is made from the plot as the filter takes into account the calculated conductor temperature values from both the methods and give a more precise estimate of conductor temperature.

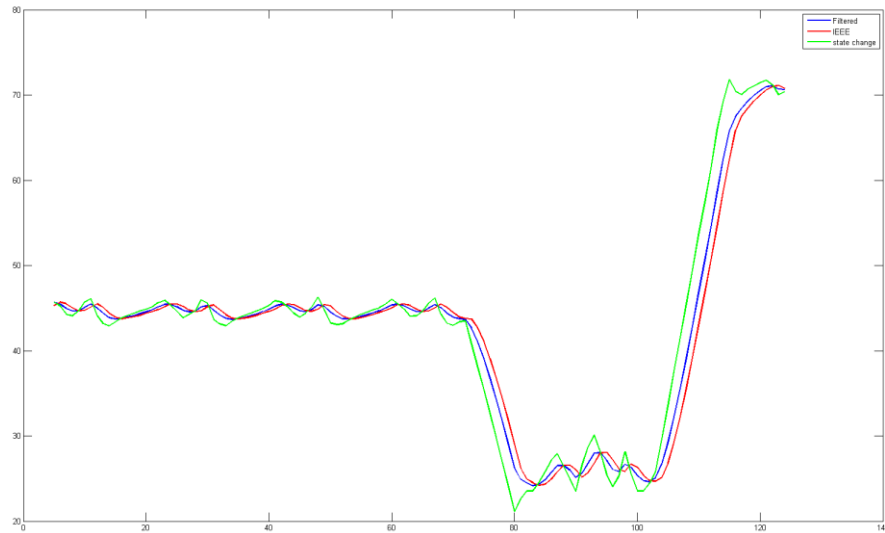


Figure 5.3 Kalman filter effect

Chapter 6

6 Instrumentation and data acquisition

The aim of this thesis work is to develop an application which based on real-time measurements provides a real-time estimate of ampacity. Hence, data acquisition in real-time is indispensable. Entire testing work has been conducted in SmarTS lab. This section of the report explains the architecture of laboratory and the procedure implemented to develop and execute the application.

6.1 SmarTS lab architecture

Figure 6.1 shows the basic architecture of SmarTS lab. The lab has a simulator which can be used perform simulations in real-time. Measurement from the model running on the simulator can be sent to PDCs or application through PMUs with high sampling rate. There are external controllers and amplifiers that can be used to send control signals to the model. In the following sections, lab equipment and application that have been used in this thesis work are explained.

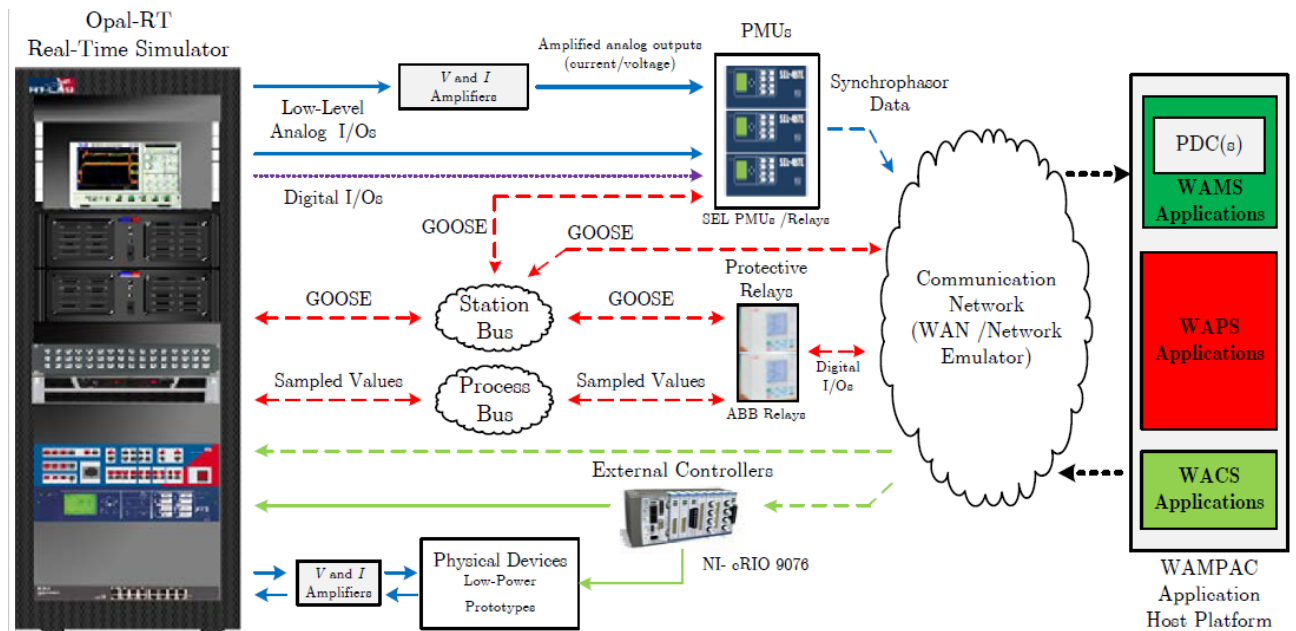


Figure 6.1 SmarTS Lab architecture

6.2 Application process

Figure 6.2 is a flow chart depicting the process which is followed to run the model and receive the real-time measurements in developed LabVIEW application. In this section, different steps (devices and applications) used in this process are explained in detailed.

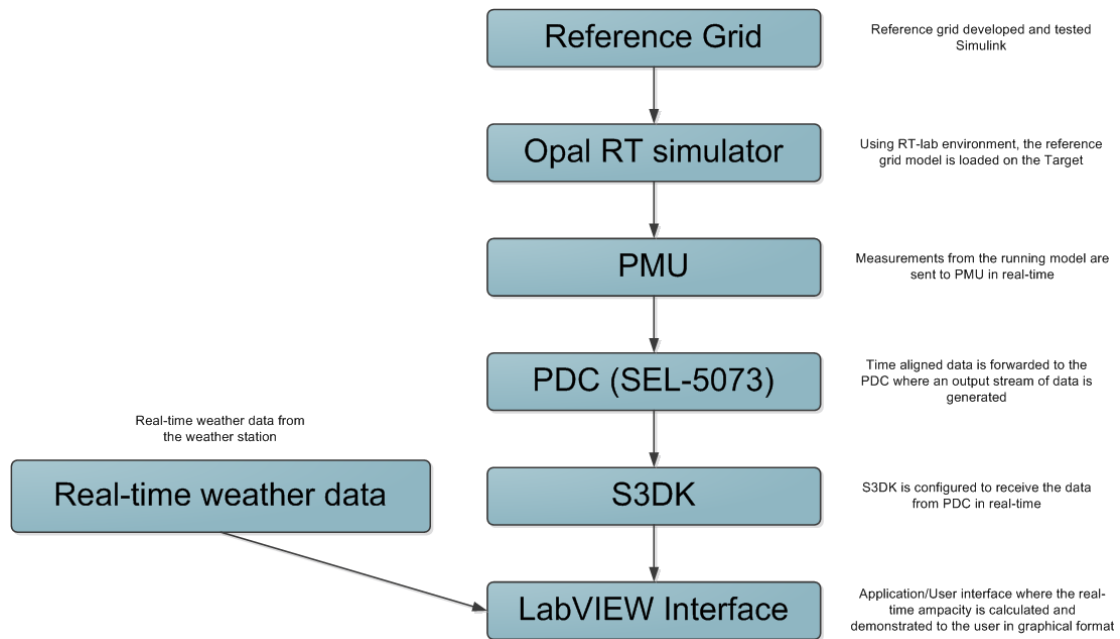


Figure 6.2 Application process block diagram

6.2.1 Reference grid

Reference grid is the model which is used to test the developed application. The reference grid model introduced in [17] was developed in MATLAB/SIMULINK and RT-LAB environment. Using the libraries of RT-LAB it is possible to send the measurements to the output of simulator. The reference grid consists of 12 sub-systems as can be seen in the Figure 6.3. There is 1 master system, 11 sub-systems and a console where results can be seen while the model is running. The model usage is explained in detail in the next chapter.

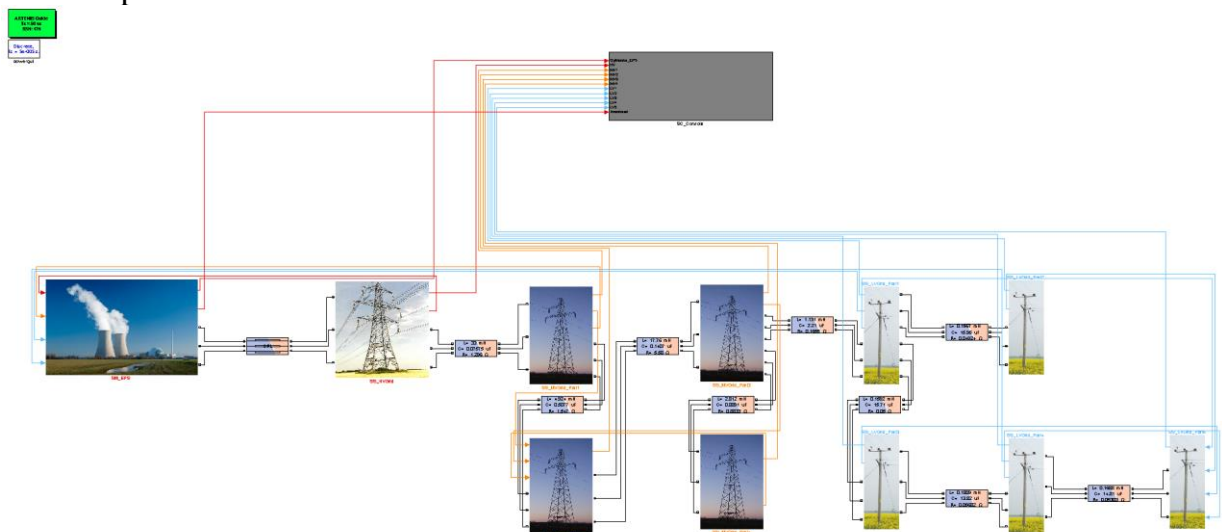


Figure 6.3 Reference Grid SIMULINK model

6.2.2 Opal RT simulator

The Opal RT simulator consists of one master chassis and one extension chassis. Figure 6.4 is a picture of actual simulator. The master chassis, ML605 FPGA has Xilinx ML605 development boards are based on a Virtex-6 processor which has the main use for floating point models and projects which have large on-board memory requirements. The master chassis has an operating system (REDHAT-LINUX). It has 12 computation cores and provides synchronization signals to the slave and takes care of its own I/Os and keeps track of over-runs.

On the other hand the extension chassis, OP 5142 FPGA is a user configurable FPGA based I/O board based on Xilinx Spartan-3, and is ideal for fixed-point models using on-board memory. It provides more I/Os and synchronizes them with the master chassis.



Figure 6.4 Opal RT Simulator

Table 6.1 enlists the specifications of RT simulator. It can be seen that each chassis consists of 12 cores. Therefore, ideally a model can be subdivided in 12 sections or 24 cores depending on whether one chassis is being used or to. Each section of the model is then automatically assigned to one core and thereby providing faster execution of the model. The sub-system division of the reference grid can be seen in Figure 6.3.

Table 6.1: Simulator specifications

Features	Detail
Number of cores	24 (12 * 2)
Analog inputs	32 (± 10 mA and ± 100 V)
Analog outputs	96 (± 10 mA and ± 100 V)
Digital inputs	128 (± 4 V to ± 30 V and 60 mA)
Digital outputs	128 (± 4 V to ± 30 V and can sink up to 100 mA current)
High voltage DC interface	16 digital outputs (250 V DC and up to 125 A current)

6.2.3 Phasor Measurement Unit

Phasor measurement unit is device used to measure electrical signals with time synchronization. Figure 6.5 shows SEL-412 relay which is being used as a PMU for this application. It provides measurement at a high sampling rate.



Figure 6.5 SEL-421

The PMU measures the required quantities from the running model in real-time which are further used in LabVIEW application.

The connection between the simulator's analog outputs and the PMU is made through DB37 breakout board. These boards bring all 37 pins of a DB37 connector out to screw terminal blocks for easy connection and prototyping work. BRK37M has a male connector. These boards are ideal for experimentation and prototype works. Figure 6.6 shows an image of actual DB37 board. Further specifications can be found in the **Appendix B**.

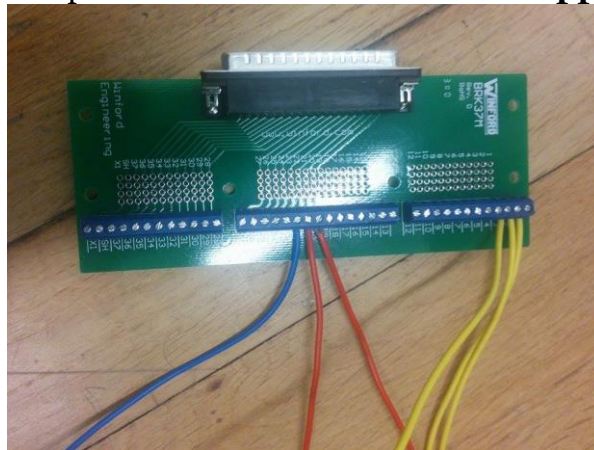


Figure 6.6 BRK37M board

6.2.4 Phasor Data Concentrators

Figure 6.7 shows a simple structure of synchrophasor network consisting of several PMUs and PDCs. The arrow from PMU to PDC indicates the PDC input stream. In a typical network many PMUs are located at various key positions; measurements from these PMUs are sent to PDC in real-time where the data is aggregated together for further processing [32].

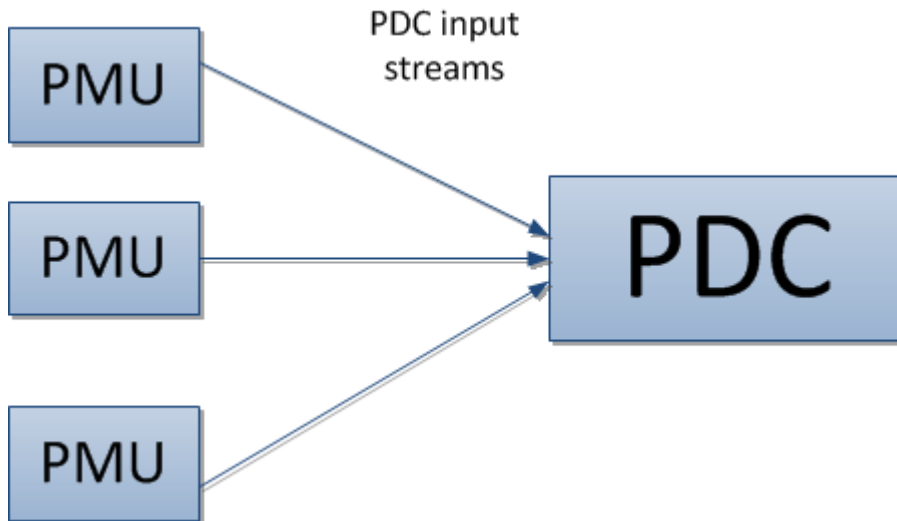


Figure 6.7 Synchronphasor data collection network

SEL-5073, available from <https://www.selinc.com/SEL-5073/> is software which connects to any IEEE C37.118-2005 compliant PMU. To add an output stream, a menu is available in the left menu window as shown in Figure 6.8. To create a new stream the inputs of output name, PDC ID, Data rate, waiting period, Transport protocol, Port no. and Local IP address are to be specified here. This stream can then be directly tested in PMU connection tester and received in real-time in the LabVIEW application.

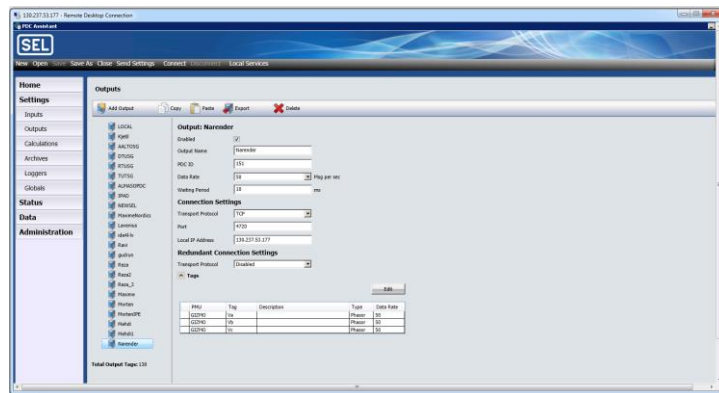


Figure 6.8 SEL-5073 Synchronwave output

6.2.5 PMU connection tester

The PMU connection tester is software administered by the Grid Protection Alliance (GPA) that verifies that a data stream from synchrophasor device is being successfully received. The software is available from <https://pmuconnectiontester.codeplex.com/>.

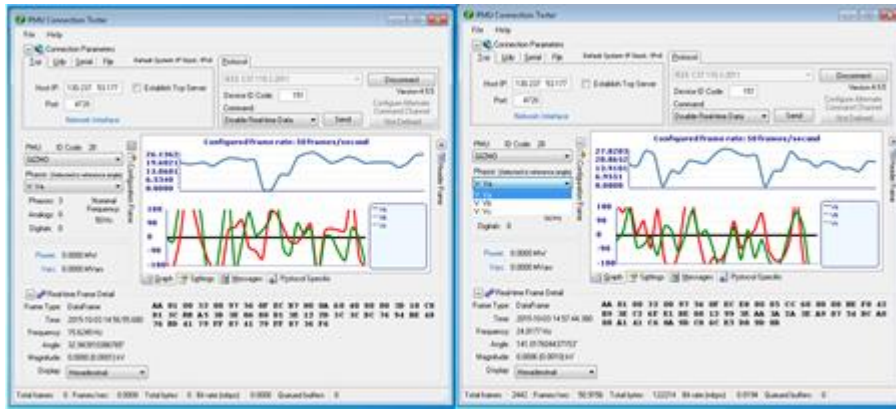


Figure 6.9 PMU connection tester

The main window of PMU connection tester can be seen in Figure 6.9. It can be used to test various devices like PMU, PDC, Digital Fault recorder and Power Quality Meter (PQ). Although for the purpose of this thesis, it has been used to test PMU and PDC connections.

6.3 S³DK

In order to connect the incoming data stream from the PMU to the LabVIEW application, S³DK is used. It communicates with PMU or the PDC using IEEE C37.118.2 protocol [33].

S³DK can be activated from the front panel once the application is running. On checking PRL visible option, Figure 6.10; the S³DK interface will appear as can be seen in Figure 6.11.

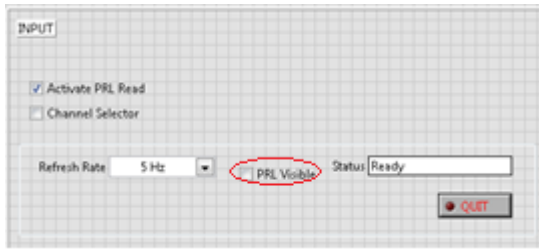


Figure 6.10 S3DK interface

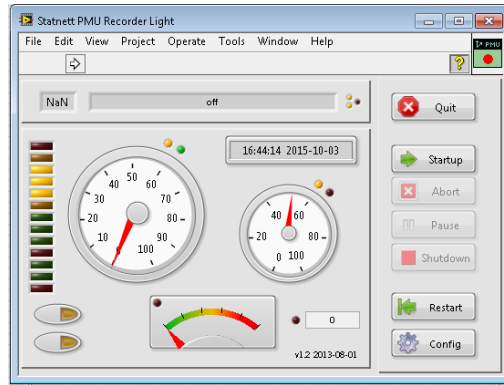


Figure 6.11 S3DK activation

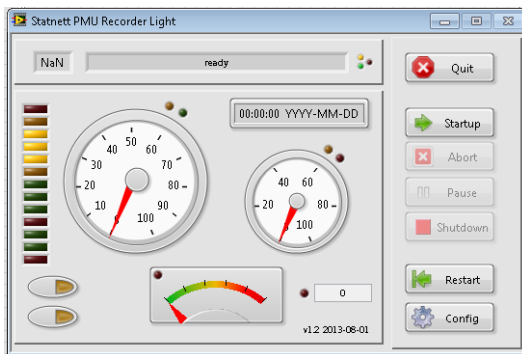


Figure 6.12 Configuration

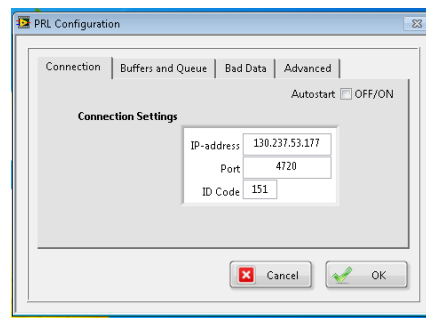


Figure 6.13 Running S3DK

When the connection to PMU is verified with PMU connection tester, the connection parameters are entered using S3DK configuration as shown in Figure 6.13. The first tab is connection where IP- address, Port and PDCID of the connection are entered. When the connection is active, the Pause and Shutdown buttons are activated and the indicator will show activity which indicates that the data is available and can be retrieved from the access buffer.

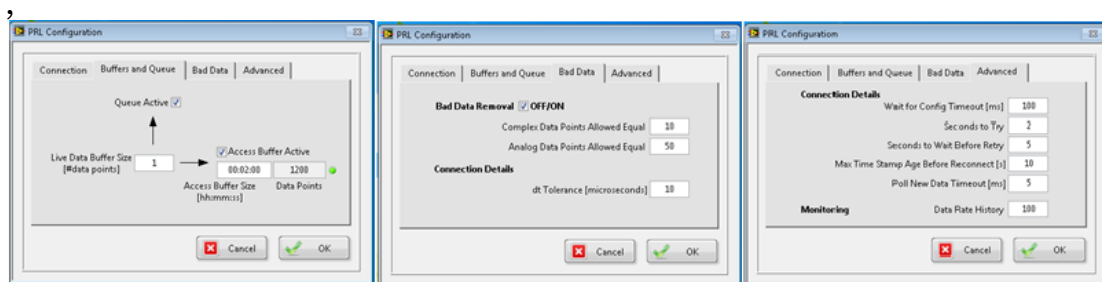


Figure 6.14 Buffer and Queue, Bad Data, Advanced

Figure 6.14 shows the Buffer and Queue, Bad Data and Advanced tabs of S3DK configuration. The data buffer size determines the number of data frames that will be read from the incoming data before the data is passed on the Access buffer or the output queue. Access buffer size determines the amount of data made available to the application.

Data points indicate the actual amount of data frames contained in the Access buffer. When a signal is missing, the phasor or analog frequency signal coming from the PMU is difficult to determine the validity of signal. Hence, the

software is set to compare succeeding data points, and if enough of them are equal, the signal is treated as invalid, and data is replaced with Nan. From the advanced settings further settings can be done.

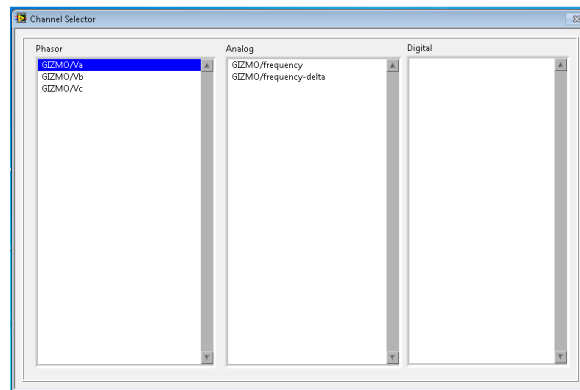


Figure 6.15 S3DK Channel Selector

The S3DK channel selector shown in Figure 6.15 is used to select the data stream which is needed for the application. The channels appear in order of output of the read buffer. These data streams can then be received in real-time and be fed to the algorithm for ampacity calculation.

6.4 Real-time weather data

Real-time weather data is critical for the algorithm to work. Therefore, LabVIEW interface was used to directly connect to a weather station and receive regularly updated measurements. Figure 6.16 shows the application that has been developed to receive weather data in real-time. The application works on the reference of time scale that is received from the PDC, hence all the measurements in this application are time aligned. In the top part of this application there are three digital indicators that display the latest wind direction, ambient temperature and wind speed. Whereas, the lower part of this application shows the measurement of ambient temperature and wind speed in graphical form, these are the measurements being used in ampacity calculation.

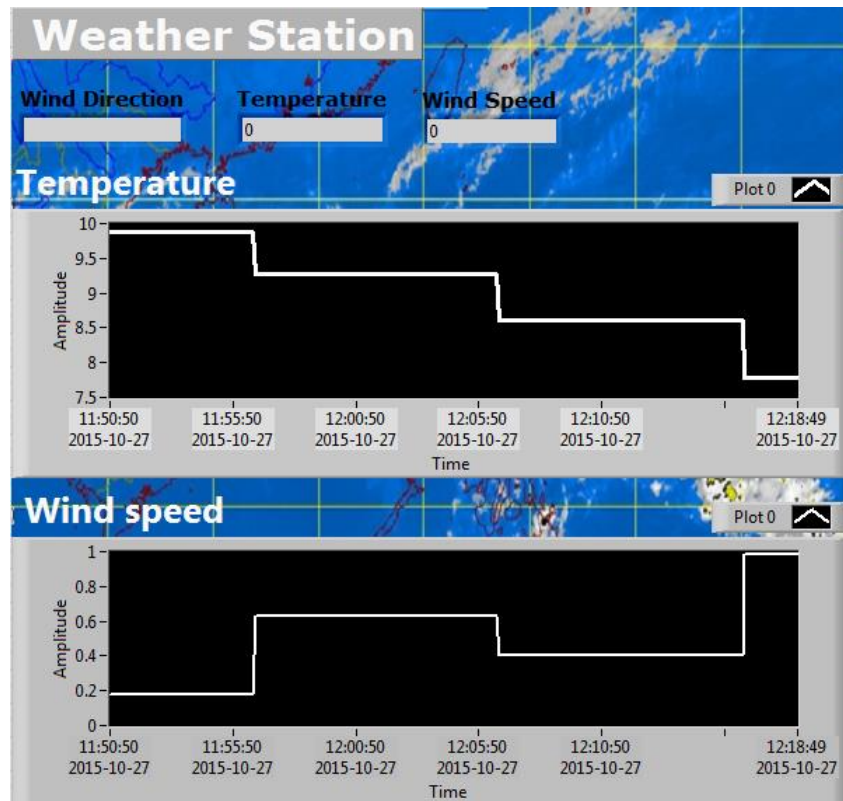


Figure 6.16 Application for receiving weather data

6.5 LabVIEW application

Figure 6.17 shows the entire GUI or as called in LabVIEW language, the front panel of the developed application. The application is divided into different segments. The top left corner of the application is dedicated to the display of the weather measurements that are received in real-time. The bottom left portion of the front panel displays the sag level of the conductor span that is under monitoring.

The segment of front panel on the right side is dedicated to the conductor measurements/estimates and properties. The top portion in this segment is the only part in the whole application which is control based. This part can be controlled by the user to change the conductor parameters depending upon the type of conductor. Other waveforms of line ampacity, line loading and conductor temperature are also present in this section. These are updated in real-time as soon as new data is received.

It should be noted that all these waveforms have a common time scale of the time that is received from the PDC. This makes it easy for the user to compare the waveforms and see the effect of changing conditions on the line ampacity.

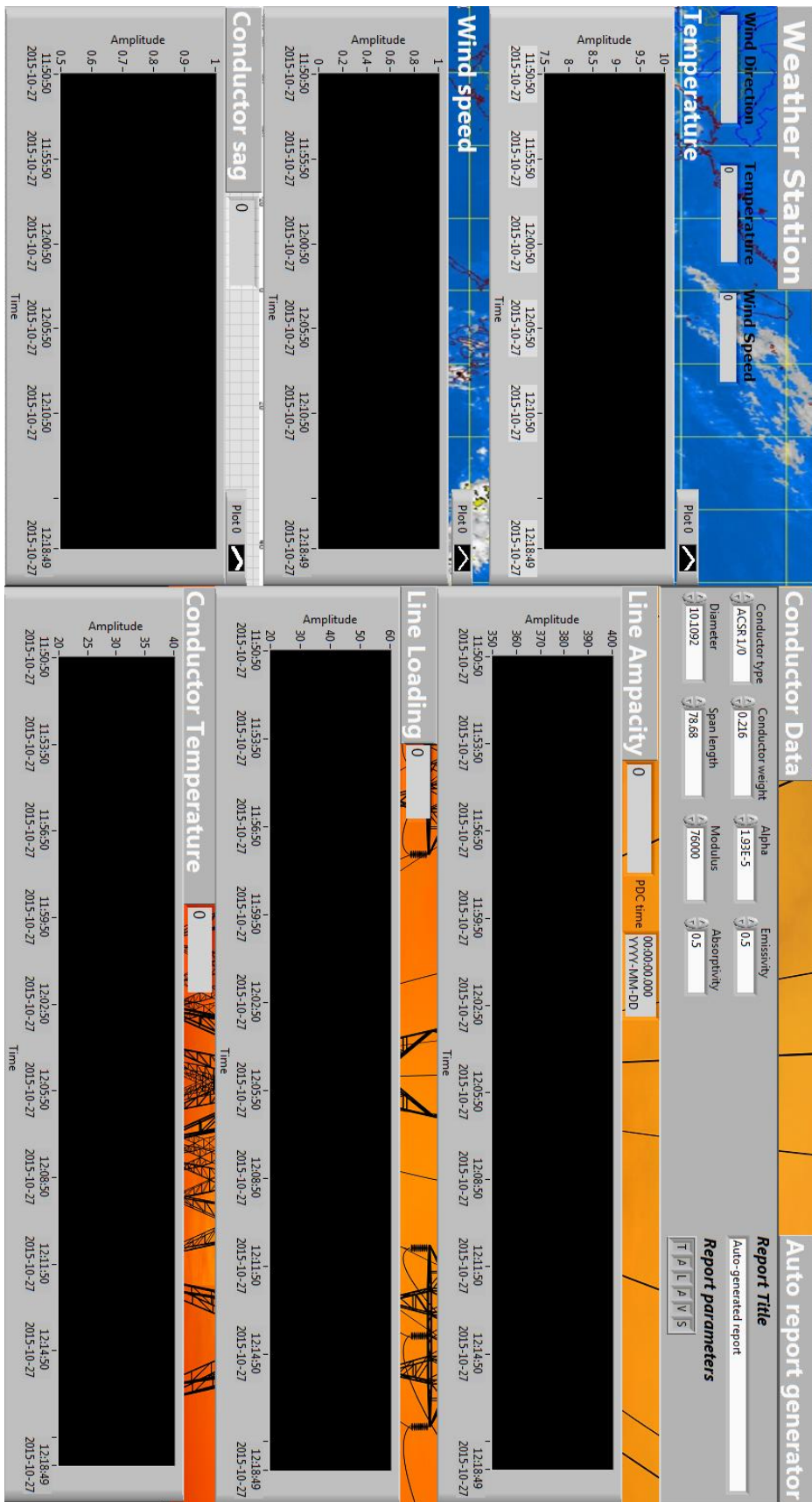


Figure 6.17 LabVIEW application

6.5.1 Auto-generated report

A very useful part of this application is the auto-generated report. The controls for this are provided on the top right corner of the front panel. As soon as the application stops running, an excel sheet is generated automatically. This data can later be used for analysis. Table 6.2 shows a sample auto-generated report

Table 6.2 Auto-generated report

<i>Time</i>	<i>Ampacity</i>	<i>Line Loading</i>	<i>Ambient Temperature</i>	<i>Wind Speed</i>	<i>Sag</i>	<i>Conductor Temperature</i>
13:17:04	309,187706	24,876013	6	0,357632	1,028876	44,070825
13:17:41	313,020114	30,260082	6	0,357632	1,008872	42,928779
13:17:46	311,501182	28,005423	6	0,357632	1,016558	43,381837
13:17:52	309,822521	30,425911	6	0,357632	1,024487	43,881898
13:17:57	309,158027	29,761816	6	0,357632	1,027571	44,079655
13:18:03	308,349654	30,547365	6	0,357632	1,031376	44,320084
13:18:08	307,309752	29,505775	6	0,357632	1,036272	44,629132
13:18:14	306,61329	27,707108	6	0,357632	1,039523	44,835959
13:18:21	305,43161	28,962948	6	0,357632	1,04507	45,18659
13:18:28	303,361799	29,287058	6	0,357632	1,054772	45,799853
13:18:37	304,462648	29,303343	6	0,357632	1,049474	45,473827
13:18:43	307,011243	28,876596	6	0,357632	1,037499	44,717795
13:18:49	309,58444	27,884493	6	0,357632	1,025407	43,952765
13:18:55	308,779403	28,62631	6	0,357632	1,029355	44,192288
13:19:01	306,798865	30,269203	6	0,357632	1,038713	44,780861
13:19:07	303,383927	30,247896	6	0,357632	1,054741	45,793303
13:19:12	303,119286	27,929821	6	0,357632	1,055828	45,871631
13:19:18	309,143065	27,789995	6	0,357632	1,027323	44,084107
13:19:24	312,037772	30,237947	6	0,357632	1,013812	43,221849
13:19:30	313,0476	30,234838	6	0,357632	1,00912	42,920576
13:19:35	311,551823	28,04838	6	0,357632	1,016316	43,366741
13:19:41	310,069425	28,551899	6	0,357632	1,023309	43,80839
13:19:48	308,92649	30,23893	6	0,357632	1,028674	44,148537
13:19:53	308,184822	28,818041	6	0,357632	1,03215	44,369089
13:19:59	307,380047	27,713823	6	0,357632	1,035931	44,60825
13:20:05	306,369907	29,01144	6	0,357632	1,040678	44,908206
13:20:10	305,501338	28,850828	6	0,357632	1,04474	45,16591
13:20:16	303,986331	27,936056	6	0,357632	1,051845	45,614933
13:20:22	302,991224	28,645323	6	0,357632	1,056456	45,909528
13:20:28	304,904954	27,812675	6	0,357632	1,047392	45,342742
13:20:34	307,273738	27,791344	6	0,357632	1,03628	44,63983
13:20:40	309,795413	29,003115	6	0,357632	1,024415	43,889968
13:20:46	308,667299	30,175598	6	0,357632	1,029899	44,225629
13:20:51	306,507236	28,916021	6	0,357632	1,040088	44,867442
13:20:57	303,141628	29,578239	6	0,357632	1,05587	45,865019
13:21:03	303,488385	30,385719	6	0,357632	1,054079	45,76238
13:21:09	309,914443	30,150362	6	0,357632	1,023669	43,854533
13:21:15	312,201194	30,211735	6	0,357632	1,013066	43,173109
13:21:20	312,975425	28,750578	6	0,357632	1,009473	42,942116

7 Testing and Results

7.1 Test model

The application developed in this thesis has been tested on the reference grid [17]. Similar to this thesis, the model was also developed as a part of project IDE4L project [34]. Using this model it is possible to perform real-time hardware-in-the-loop simulations. The result from this model has been used as real-time input to the developed application.

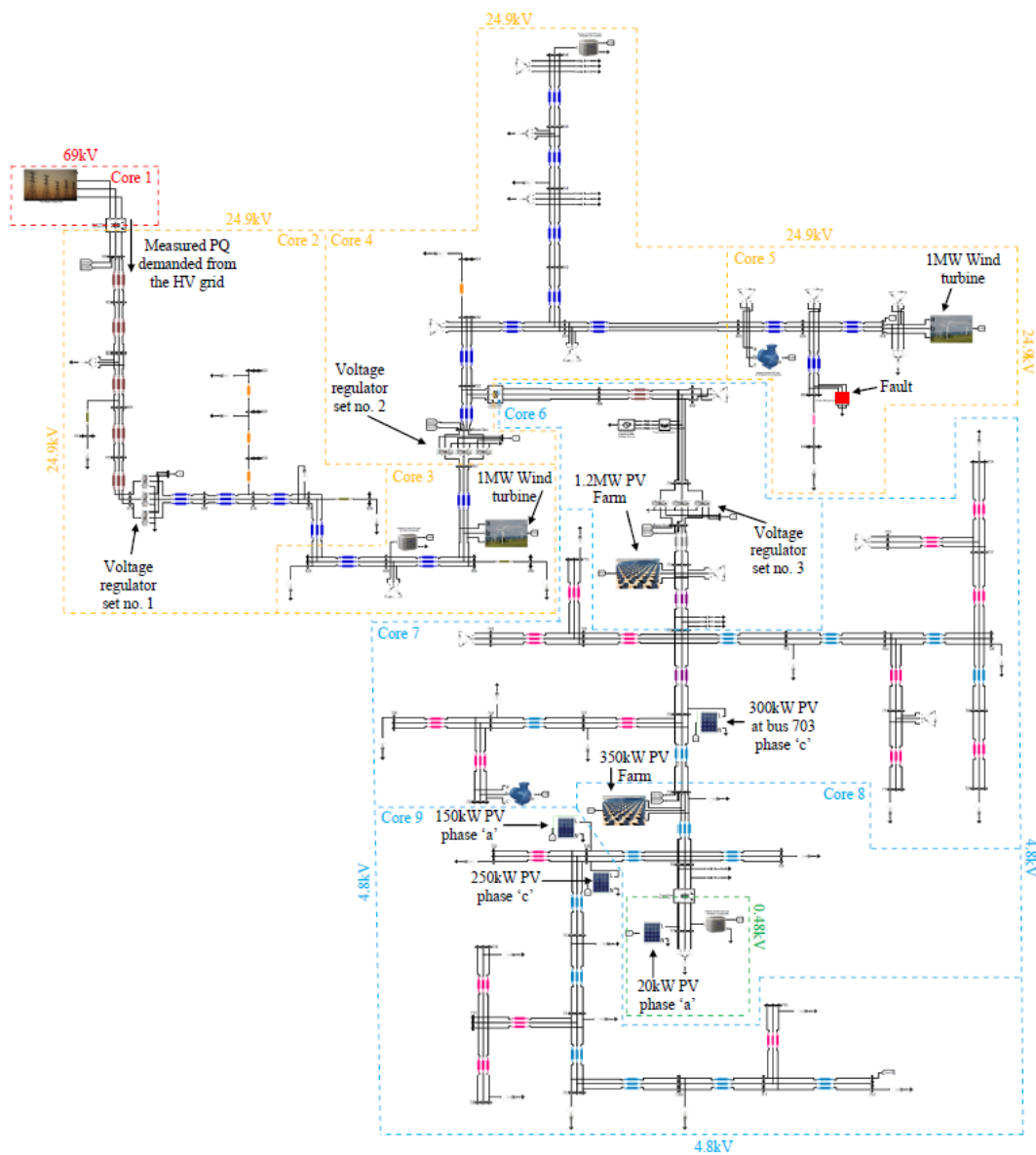


Figure 7.1 Reference grid model

Figure 7.1 shows the test model reference grid. The topology of this grid model is based on different IEEE standard test feeders including HV, MV and LV voltage levels. Details of this model are provided in [17]. To run the test, Reference Grid model is implemented in OPAL-RT software. The model is then loaded and simulated on a real-time simulator; this simulator then sends desired signals to a PMU in real-time to be used in the application.

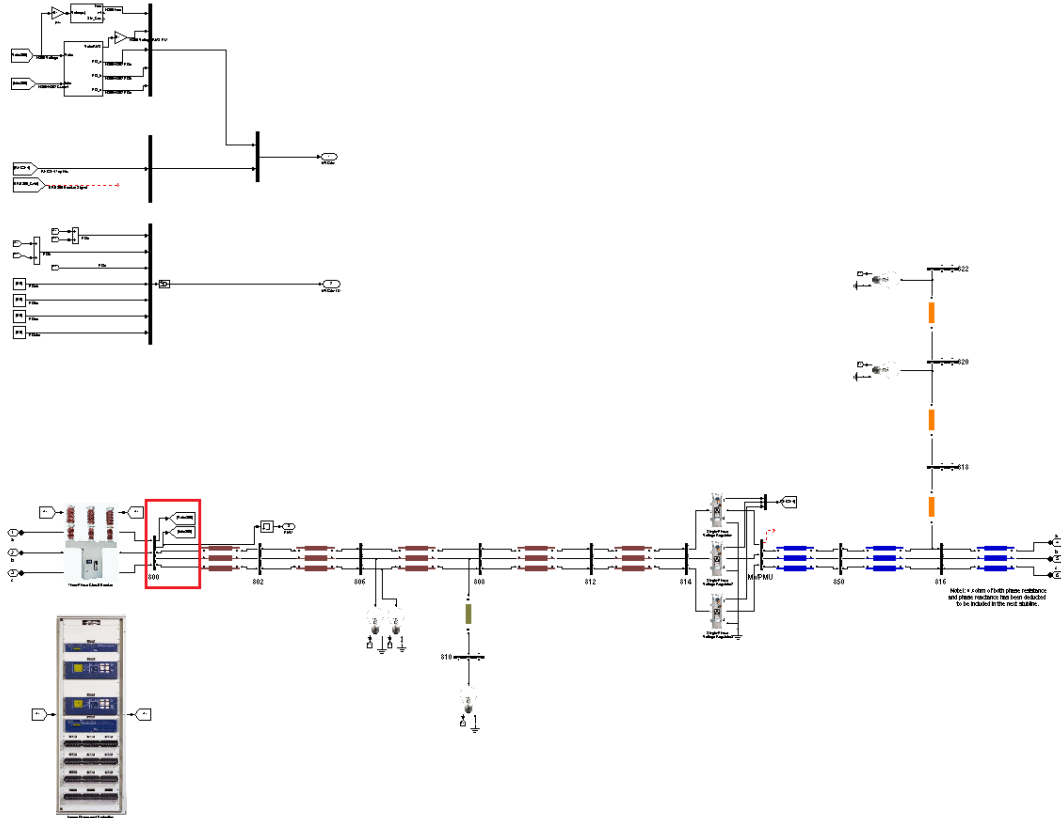


Figure 7.2 Medium voltage part of reference grid

It can be seen from Figure 7.1, Reference Grid is an extensive model consisting of sections having low voltage, medium voltage and high voltage level. For testing purpose the medium voltage part was chosen. Figure 7.2 shows a sub-section of medium voltage section. The line section which has been tested for calculation of DLR is the section from bus 800 to bus 802; this is shown in a red box in the Figure 7.2.

This section of the reference grid is based on IEEE 34 bus feeder. The line configuration type of this section is 300. The specifications of this configuration can be seen in the Table 7.1.

Table 7.1: Overhead line configuration

Configuration	Phasing	Phase	Neutral	Spacing ID
		ACSR	ACSR	
300	B A C N	1/0	1/0	500
301	B A C N	#2 6/1	#2 6/1	500
302	A N	#4 6/1	#4 6/1	510
303	B N	#4 6/1	#4 6/1	510
304	B N	#2 6/1	#2 6/1	510

7.2 Results

The final result of the developed application is demonstrated in this section. The results here are shown in graphical form as a part of front panel of the application developed in LabVIEW environment. As has been discussed, the ampacity of an overhead line is influenced mostly by the change in conductor sag and the ambient weather conditions. Therefore, the results are shown in two different parts. The first part of results demonstrates the combined impact of change in sag, weather conditions and line loading, and how it affects the ampacity of the line. In the next sub-section the impact of variation in weather on line ampacity is demonstrated.

7.2.1 Impact of weather, line loading and sag on line ampacity

Figure 7.3 demonstrates the combined impact of weather, line loading and sag on line ampacity. The image is a direct screenshot of the front panel of the application developed in LabVIEW.

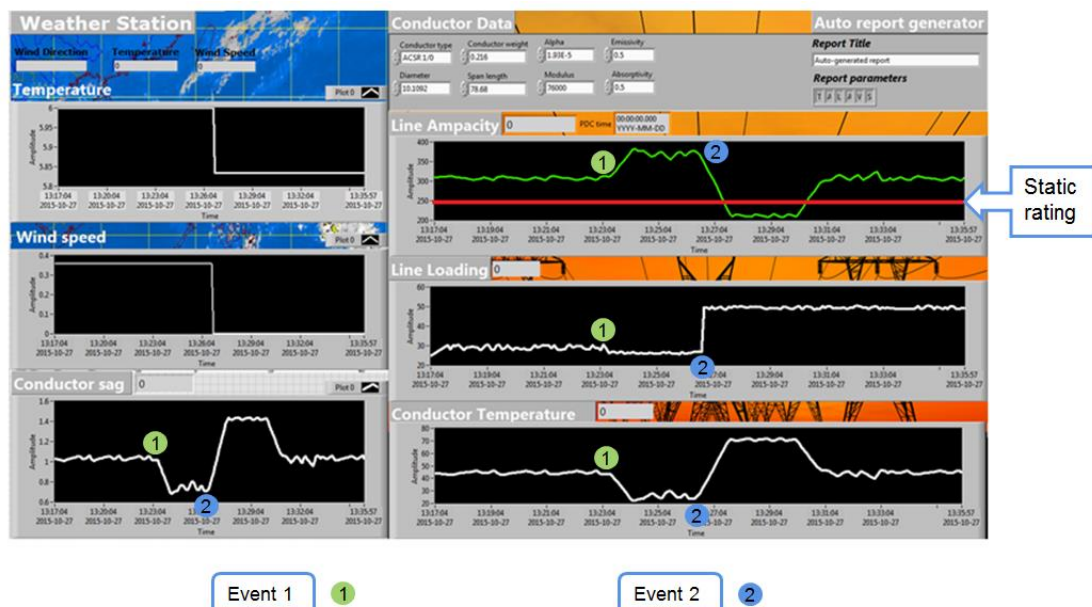


Figure 7.3 Impact of weather, line loading and sag on line ampacity

The simulations were conducted for a period of time that was sufficient enough to clearly see the impact of changing conditions on the line ampacity. The left portion of the Figure 7.3 represents the weather station and sag monitoring section of the application. Here, the measurements received in real-time are displayed in a graphical format.

The right portion of Figure 7.3 displays the line loading measurements which are received from the simulator in real-time and the effect of these changing conditions on conductor temperature and thereby on the line ampacity.

It can be seen in the result that at some point the line loading registers a sudden rise; this is when in the reference grid model [17] which has been running simultaneously to give real time measurements gets wind power introduced in one of the medium voltage section causing a sudden change in line current. As a result of this sudden change in the line loading a change in

sag is seen. The sag increases gradually in the form of a ramp reacting to the sudden change in line loading. A corresponding effect on the conductor temperature can also be seen here. The conductor temperature change depends on its heat capacity among other things; hence the same amount of increase in line loading can have a different impact on another kind of conductor. Also, the change in conductor temperature is not sudden rather it is a gradual change depending on the conductor material properties.

It should be noted that according to the data sheet of the conductor [Appendix B] analyzed here, the static rating of the conductor is 242 A. These ratings are based on a conservative estimate of 75°C conductor temperature, 25°C ambient temperature, 2ft/s wind speed and 96 watts/sq. foot solar radiation. The effect of using real-time measurements instead of conservative estimates can be seen in the results shown in Figure 7.3. It is clear that the ampacity calculation made with actual real time measurements gives a higher ampacity on most occasions as compared to the static rating except for the duration from time t = 13:28:00 to 13:29:40, when the high conductor sag causes the ampacity to reduce.

There are two main events in these results which are indicated in the Figure 7.3. Event 1 is when there is outage of a line in the system which results in reduced current. Consequently, sag and conductor temperature also increase resulting in higher line ampacity. On the other Event 2 happens when wind generation in one of the medium voltage section goes out which causes a reduced generation and a higher current. This high current results in increased sag and conductor temperature thereby reducing the line ampacity.

7.2.2 Impact of weather variation

Weather conditions unlike the line current do not change all of sudden. Change in weather condition is consistent but it is also gradual. The results demonstrated in the previous section contained the combined effect of various factors affecting the line ampacity, hence the impact of weather variation was somewhat overshadowed by the other influencing factors.

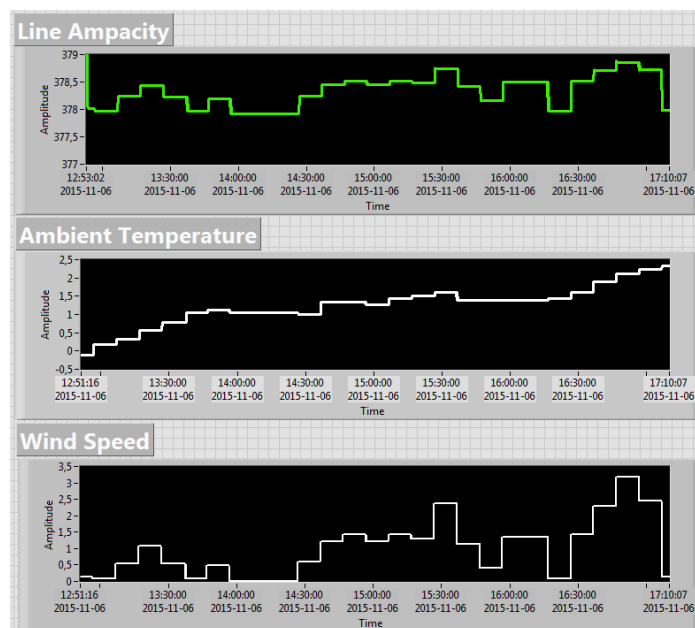


Figure 7.4 Impact of weather variation

Figure 7.4 shows the result of simulations that were performed just to see the impact of weather variation on line ampacity. To see the effect of changing weather condition on line ampacity it was necessary to run the simulation for a longer period of time, therefore these simulations were made for almost 4 and a half hours (from time $t = 12:51:16$ to $17:10:07$). For conducting these simulations the line loading and conductor sag were held constant. The application here was running in semi-online mode which means that the only real-time measurements that were used were the measurements of weather conditions. In the line ampacity chart on top in Figure 7.4, the effect of changing weather conditions can be seen. Towards the end of the chart it can be seen that the ampacity drops, this is a result of corresponding decline in the wind speed. Decline in ambient temperature on the other hand has a reverse impact on the line ampacity.

8 Conclusion and future work

8.1 Conclusion

As discussed in the beginning of this thesis, the demand of electricity is increasing. DLR systems can help increase the capacity of existing lines with very low investment as compared to the investment required to install new lines or line upgradation. Such large capital investments can be deferred by improving existing line capabilities reliably.

The thesis work presented in this report has the main objective of developing and testing an application in LabVIEW environment that can receive various inputs provided to it; be it the data stream of measurement coming from PDC, weather conditions received in real-time from a weather station or conductor data based on the type of conductor being assessed.

Although there are many DLR systems available those are being successfully implemented. There is very little focus given to optimum use distribution network using DLR. Therefore, this thesis work is developed keeping a distribution network in mind and has been tested exclusively on a distribution system model [17]. From the results it is clear that the changing conditions have significant impact on line rating.

After initial literature review for this thesis work it was important to make a decision on the method that should be used for ampacity calculation. Amongst many options IEEE 738 standard [8] was chosen as it has been tested and is being used for many DLR applications. The elaborate standard acknowledges various factors that can influence the thermal rating of an overhead conductor like solar radiation, wind speed, etc. This method has been explained elaborately in Chapter 3.

The second method used to estimate the conductor temperature in this thesis is the 'state change equation'. Unlike the elaborate IEEE standard [8], this method works directly on measurements of sag from the actual conductor span.

A distribution network model was an essential requirement to test the application developed in this thesis. An ideal model for this purpose was found in [17], it is an elaborate model of distribution network consisting of different type of load present in such a network.

Use of the Kalman filter is yet another crucial part which makes this work unique. The Kalman filter has shown to provide an accurate estimate of conductor temperature based on two different input temperature estimates.

As both the IEEE standard [8] and the 'state change equation' require actual weather conditions as input to work accurately, it was important to have a system which reports measurements like ambient temperature and wind speed in real-time. This was achieved data scraping in LabVIEW to get regularly updated data.

A major part in this thesis work was to get familiarized with various device and application in SmarTS lab, KTH. These devices were configured to imitate a real power system from which measurements were taken in real-time.

The main objectives of this thesis as well as all the specific objectives that were mentioned in Chapter 1 have been completed by the end of this thesis work. The end result of the work is an application that acquires and processes data in real-time from two independent sources (weather station and PMU) to give real-time ampacity of an overhead line.

8.2 Future work

There is a great potential for improvement in reliability of DLR systems. Accuracy of the measurement devices which provide weather data can be improved for adverse weather conditions.

Also, as the line loading measurements are received from a PMU, it could be useful to examine the errors induced in PMU measurements. There are several sources of error in PMUs. A study reported in [35] has been conducted to analyze these errors. According to this study error in PMU measurements can induce huge errors in the estimation of DLR. Therefore, as a continuation to this thesis work, an algorithm can be developed which minimizes the error from PMU measurements and provides more accurate ratings.

BIBLIOGRAPHY

- [1] Deb, Anjan K. *Power Line Ampacity System: Theory, Modeling, and Applications*. Boca Raton: CRC, 2000. Print.
- [2] Bonsu, C., Krekeler, U, Heydt, G., Schilleci, J., & Agrawal, B. *Application of the Global Positioning System to the Measurement of Overhead Power Transmission Conductor Sag*. IEEE Transactions on Power Delivery, VOL. 17, NO. 1, JANUARY 2002
- [3] Ljus, M. *Dynamic line rating – Thermal line model and control*. 2013
- [4] *Dynamic line rating systems for transmission lines*. U.S. Department of energy. April 2014.
- [5] Foss, S., Maraio, R. *Evaluation of an overhead line forecast rating algorithm*. IEEE 1991.
- [6] Talpur, S.; Wallnerstrom, C.J.; Hilber, P.; Saqib, S.N., "Implementation of Dynamic Line Rating technique in a 130 kV regional network," *Multi-Topic Conference (INMIC), 2014 IEEE 17th International*, Dec. 2014.
- [7] Dale A. Douglass and F. Ridley Thrash. *Electric Power Generation, Transmission, and Distribution*, Third Edition. May 2012, 1 -42.
- [8] IEEE Standard for Calculating the Current-Temperature of Bare Overhead Conductors," in *IEEE Standard 738-2006*. Jan. 30 2007
- [9] Ruifeng Yan; Saha, T.K., "Investigation of Voltage Imbalance Due to Distribution Network Unbalanced Line Configurations and Load Levels," in *Power Systems, IEEE Transactions on* , vol.28, no.2, pp.1829-1838, May 2013
URL: <http://ieeexplore.ieee.org/stamp/stamp.jsp?tp=&arnumber=6365288&isnumber=6504806>
- [10] Oleinikova, I.; Mutule, A.; Putnins, M., "PMU measurements application for transmission line temperature and sag estimation algorithm development," in *Power and Electrical Engineering of Riga Technical University (RTUCON), 2014 55th International Scientific Conference on* , vol., no., pp.181-185, 14-14 Oct. 2014
URL: <http://ieeexplore.ieee.org/stamp/stamp.jsp?tp=&arnumber=6998196&isnumber=6998168>
- [11] Sadanandan, N.D.; Eltom, A.H., "Power donut system laboratory test and data analysis," in *Southeastcon '90. Proceedings. IEEE*, vol., no., pp.675-679 Apr1990.
- [12] Bondarenko, A.; Vasiljev, Yu.; Mekhanoshin, B.; Oreshkin, A.; Shkaptsov, V., "OHL condition monitoring and engineering solutions to cinch maximum admissible transmitting capacity," in *Condition Monitoring and Diagnosis, 2008. CMD 2008. International Conference on* , vol., no., pp.696-700, 21-24 April 2008
URL: <http://ieeexplore.ieee.org/stamp/stamp.jsp?tp=&arnumber=4580380&isnumber=4580203>
- [13] Mai RuiKun; Fu Ling; Xu HaiBo, "Dynamic Line Rating estimator with synchronized phasor measurement," in *Advanced Power System Automation and Protection (APAP), 2011 International Conference on* , vol.2, no., pp.940-945, 16-20 Oct. 2011
URL: <http://ieeexplore.ieee.org/stamp/stamp.jsp?tp=&arnumber=6180545&isnumber=6180530>
- [14] Raniga, J.K.; Rayudu, R.K., "Dynamic rating of transmission lines-a New Zealand experience," in *Power Engineering Society Winter Meeting, 2000*.

IEEE, vol.4, no., pp.2403-2409 vol.4, 2000
URL: <http://ieeexplore.ieee.org/stamp/stamp.jsp?tp=&arnumber=847185&isnumber=18389>

- [15] S. Uski-Joutsenvuo and R. Pasonen, 'Maximising power line transmission capability by employing dynamic line ratings- technical survey and applicability in Finland', 2013.
- [16] Kamboj, S.; Dahiya, R., "Evaluation of DTLR of power distribution line from sag measured using GPS," *Energy, Automation, and Signal (ICEAS), 2011 International Conference on*, vol., no., pp.1,6, 28-30 Dec. 2011.
- [17] Hooshyar, H.; Mahmood, F.; Vanfretti, L., "Specification and implementation of a reference grid for distribution network dynamics studies," in *PES General Meeting | Conference & Exposition, 2014 IEEE*, July 2014
- [18] Jupe, S.; Bartlett, M.; Jackson, K., "Dynamic Thermal Ratings: The State of Art," in *CIREN 21st International Conference on Electricity Distribution Frankfurt*, 6-9 June 2011.
- [19] Henke, R.K.; Sciacca, S.C., "Dynamic thermal rating of critical lines-a study of real-time interface requirements," in *Computer Applications in Power, IEEE*, vol.2, no.3, pp.46-51, July 1989
- [20] Davis, Murray W. System for Rating Electric Power Transmission Lines and Equipment. Patent US5140257 A. Aug. 1992. Print.
- [21] Nexans. *Page 2 of 2 Press Release Monitoring of Transmission Lines Increases Network Security and Offers Additional Capacities*. Apr. 2009. Web. Oct. 2015.
- [22] Golinelli, Elena; Musazzi, Sergio; Perini, Umberto; Pirovano, Giovanni, "Laser based scanning system for high voltage power lines conductors monitoring," in *Electricity Distribution - Part 1, 2009. CIREN 2009. 20th International Conference and Exhibition on*, vol., no., pp.1-3, 8-11 June 2009.
- [23] Ren Lijia; Li Hong; Liu Yan, "On-line monitoring and prediction for transmission line sag," in *Condition Monitoring and Diagnosis (CMD), 2012 International Conference on*, vol., no., pp.813-817, 23-27 Sept. 2012.
- [24] Ukil, A.; Braendle, H.; Krippner, P., "Distributed Temperature Sensing: Review of Technology and Applications," in *Sensors Journal, IEEE*, vol.12 May 2012.
- [25] T. Shiota and T. Wada, "Distributed temperature sensors for single mode fibers," *Proc. SPIE*, vol. 1586, pp. 13-18, 1991.
- [26] Deb, Anjan Kumar. Object Oriented Expert Power Line Ampacity System. Anjan Kumar Deb, assignee. Patent US5933355 A. Aug. 1999. Print.
- [27] IEEE Standard for Calculating the Current-Temperature Relationship of Bare Overhead Conductors," in *IEEE Standard 738-2012*, vol., no., pp.1-72, Dec. 23 2013
- [28] British Standards, "Electric cables – Calculations of the current rating", IEC 60287, British Standards, July 2002
- [29] Pinto, R.E., "State Change Equation: Calculation formula," in *Engineering Applications (WEA), 2012 Workshop on*, vol., no., pp.1-5, 2-4 May 2012
- [30] Motlis, Y.; Reding, J.L.; Seppa, T.O.; White, H.B., "Limitations of the ruling span method for overhead line conductors at high operating temperatures," in *Power Delivery, IEEE Transactions on*, vol.14, no.2, pp.549-560, Apr 1999
- [31] Welch, G. & Bishop, G. 1995. *An Introduction to the Kalman Filter*.

Technical Report. University of North Carolina at Chapel Hill, Chapel Hill, NC, USA.

- [32] IEEE Guide for Phasor Data Concentrator Requirements for Power System Protection, Control, and Monitoring," in *IEEE PC37.244 D6.0 January 23, 2013*, vol., no., pp.1-63, May 10 2013.
- [33] IEEE Standard for Synchrophasor Data Transfer for Power Systems," in *IEEE Standard C37.118.2-2011*.
- [34] <http://www.ide4l.eu>
- [35] Zhao, J. Tan, L. Wu, L. Zhan, Y. Liu, J. R. Garcia and P. D. Ewing, 'ORNL/TM - 2015/314 Electrical and Electronics Systems Research Division IMPACT OF MEASUREMENT ERROR ON SYNCHROPHASOR APPLICATIONS', *US Department of Energy*, 2015.
- [36] Vanfretti, L.; Aarstrand, V.H.; Almas, M.S.; Peric, V.S.; Gjerde, J.O., "A software development toolkit for real-time synchrophasor applications," in *PowerTech (POWERTECH), 2013 IEEE Grenoble* , vol., no., pp.1-6, 16-20 June 2013
URL: <http://ieeexplore.ieee.org/stamp/stamp.jsp?tp=&arnumber=6652191&isnumber=6652052>

Appendix A

This Appendix consists of ambient temperature, Wind speed & gust and Solar radiation for the period of January 2015 to August 2015. These graphs and data for simulation were taken from Colorado Climate Center which is located within the department of Atmospheric science of Colorado State University.

1. Ambient temperature

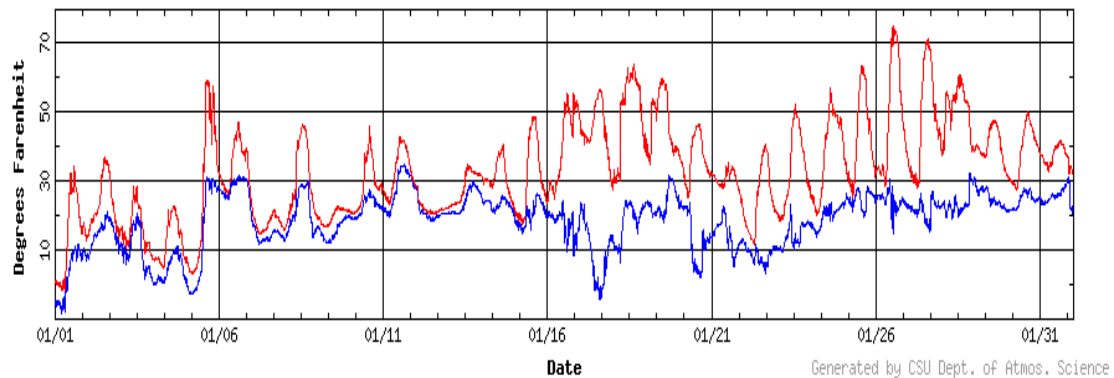


Figure A.1 Ambient temperature January 2015

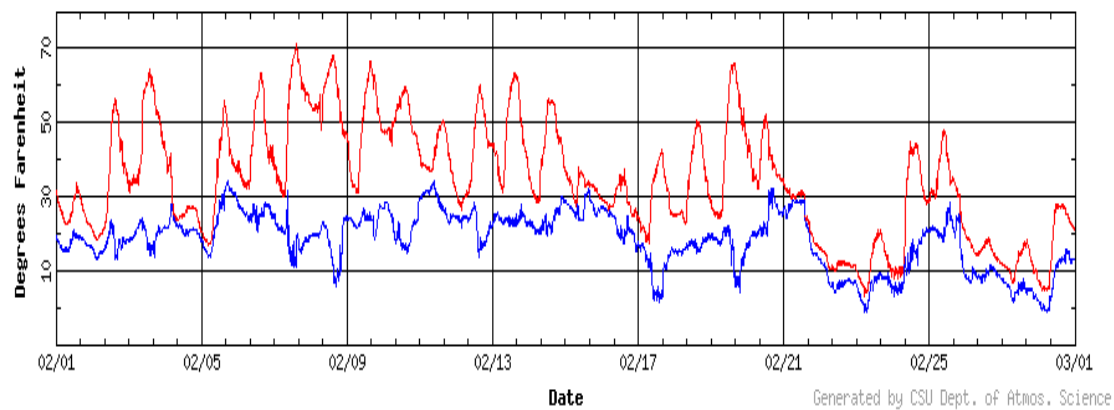


Figure A.2 Ambient temperature February 2015

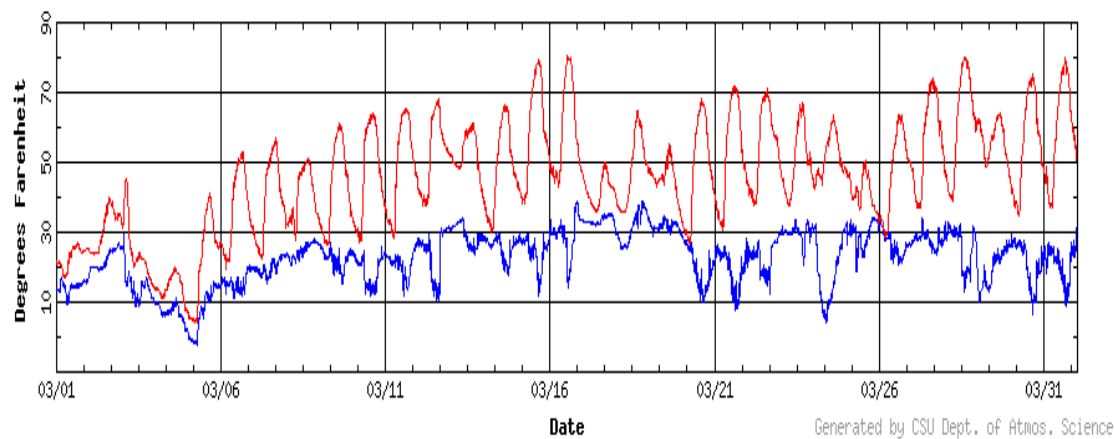


Figure A.3 Ambient temperature March 2015

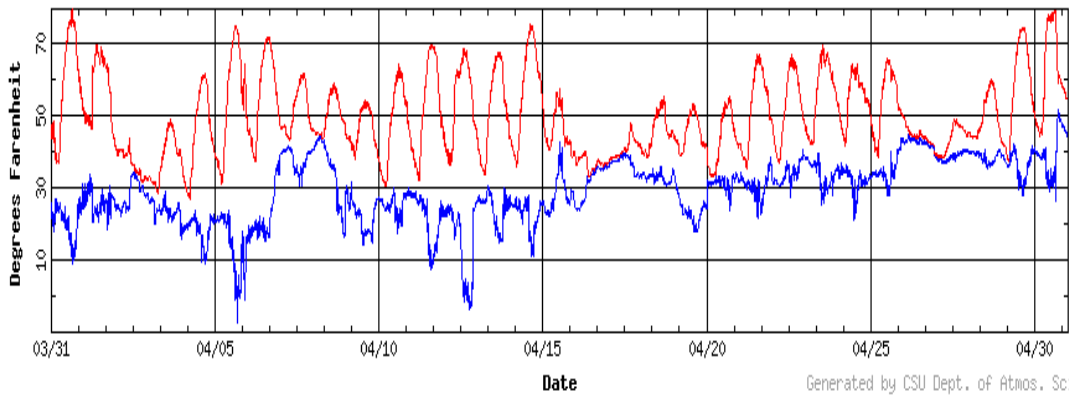


Figure A.4 Ambient temperature April 2015

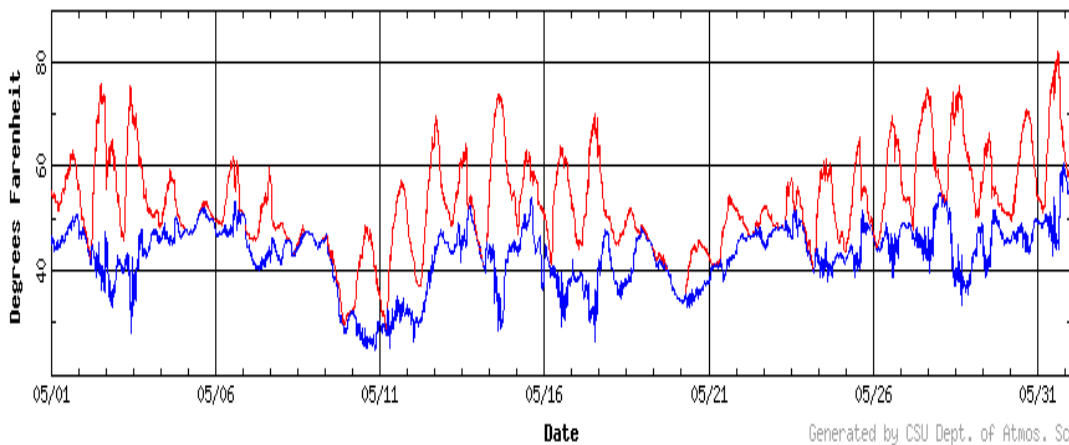


Figure A.5 Ambient temperature May 2015

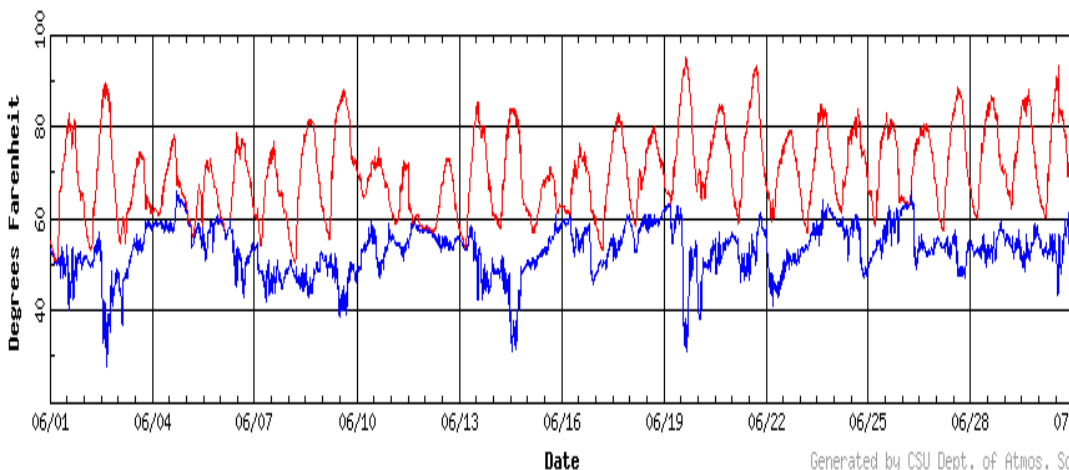


Figure A.6 Ambient temperature June 2015

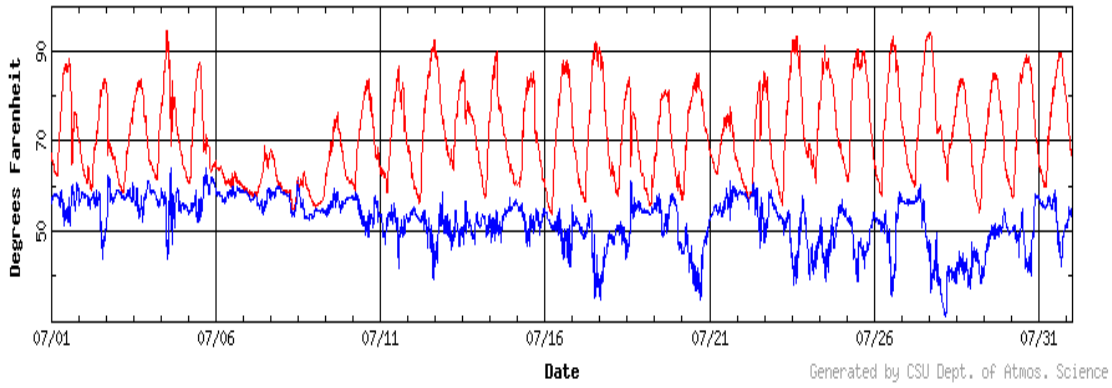


Figure A.7 Ambient temperature July 2015

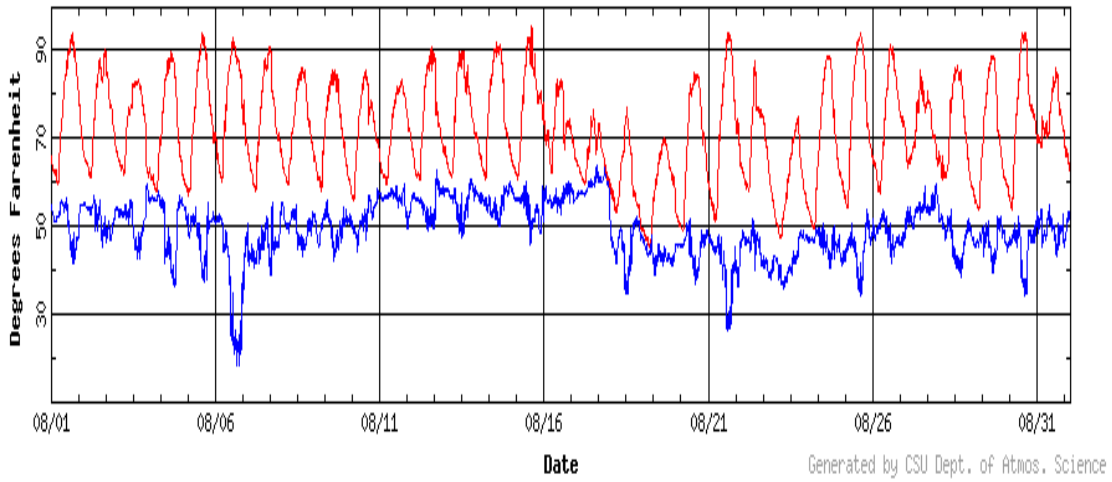


Figure A.8 Ambient temperature August 2015

2. Wind Speed and Wind Gust

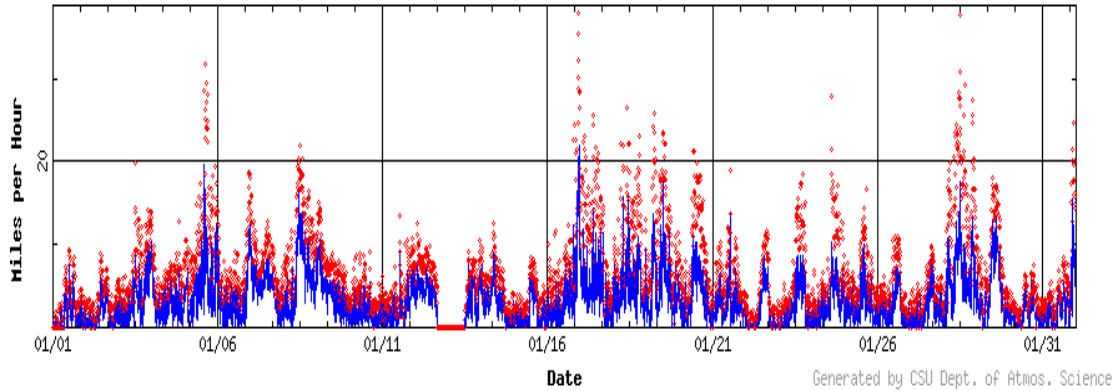


Figure A.9 Wind Speed January 2015

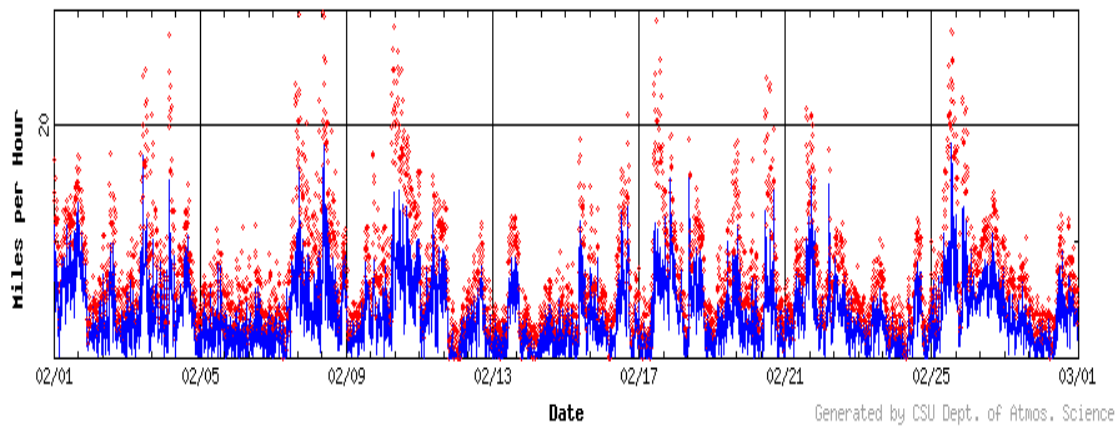


Figure A.10 Wind Speed February 2015

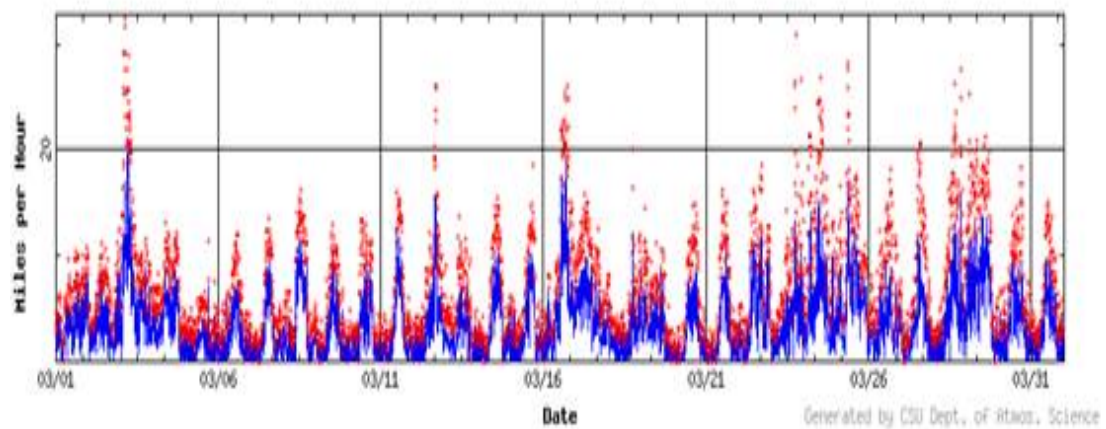


Figure A.11 Wind Speed March 2015

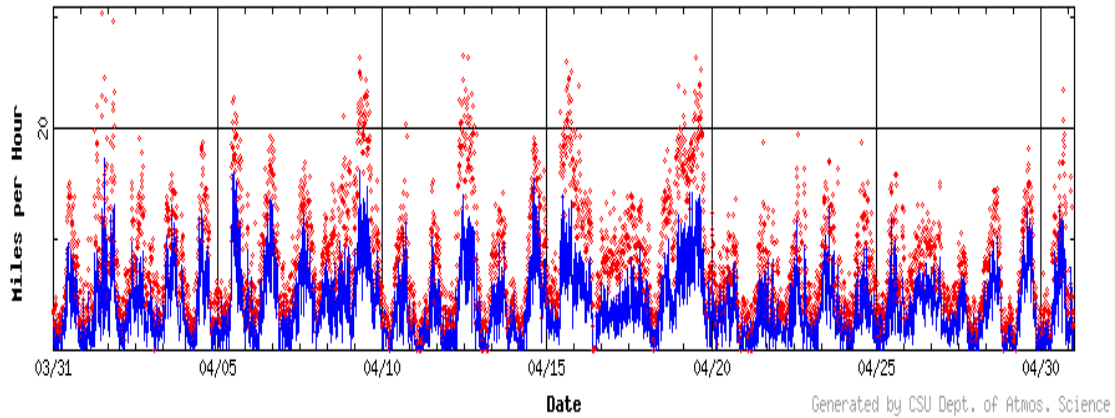


Figure A.12 Wind Speed April 2015

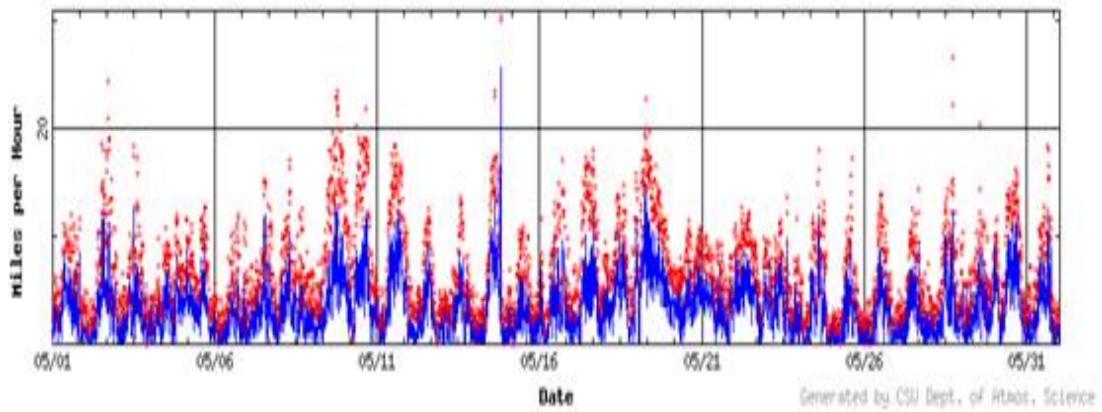


Figure A.13 Wind Speed May 2015

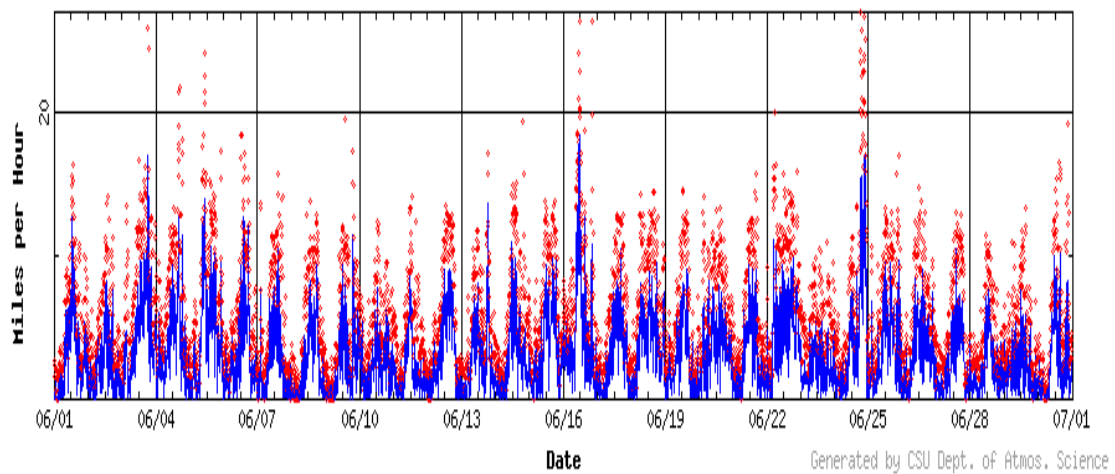


Figure A.14 Wind Speed June 2015

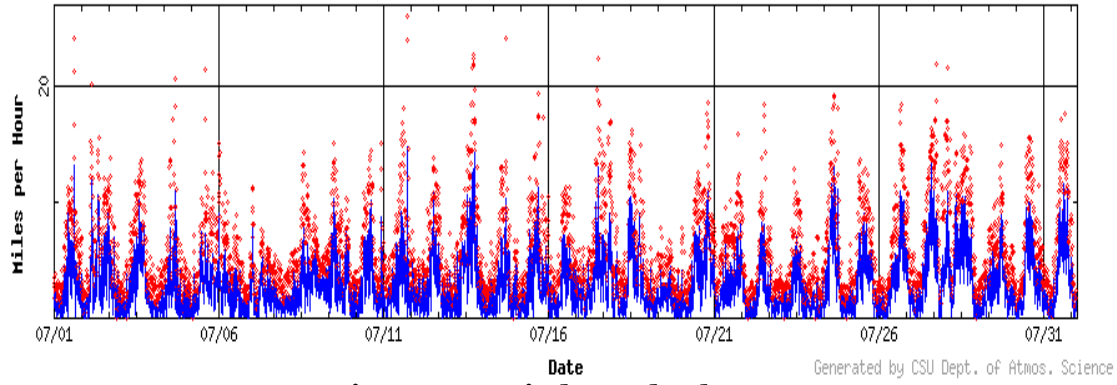


Figure A.15 Wind Speed July 2015

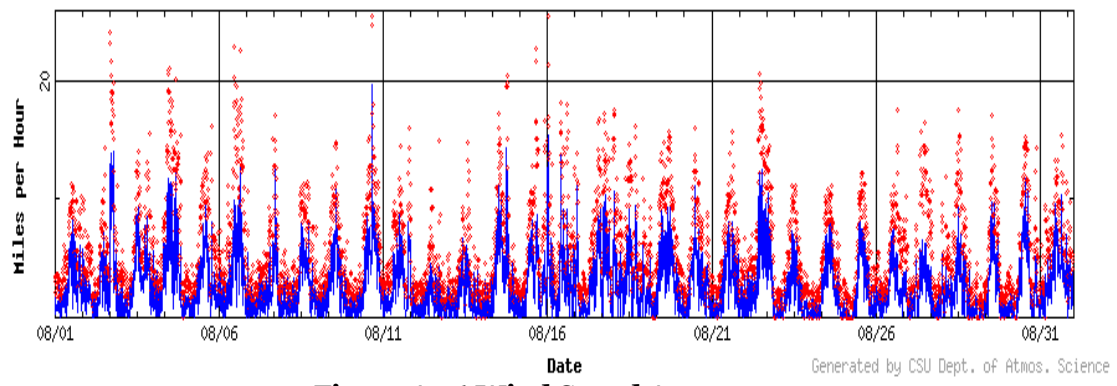


Figure A.16 Wind Speed August 2015

3. Solar Radiation

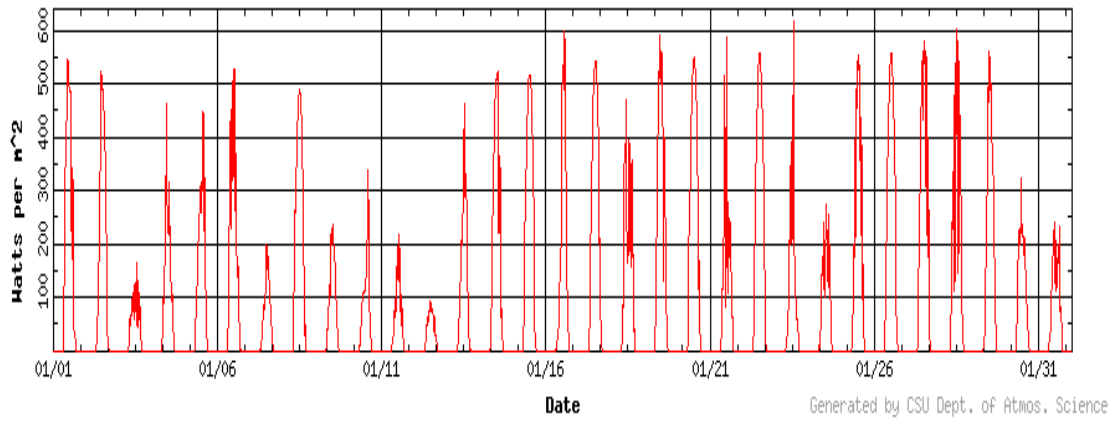


Figure A.17 Solar radiation January 2015

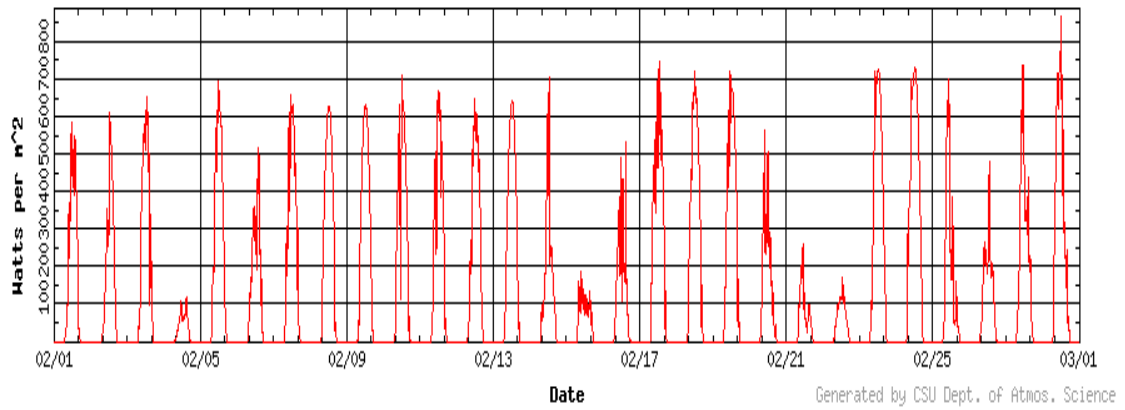


Figure A.18 Solar radiation February 2015

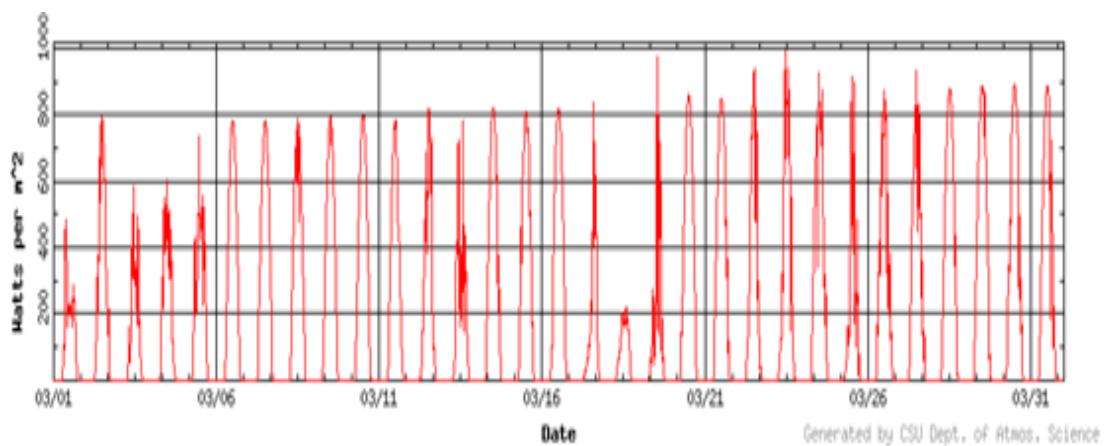


Figure A.19 Solar radiation March 2015

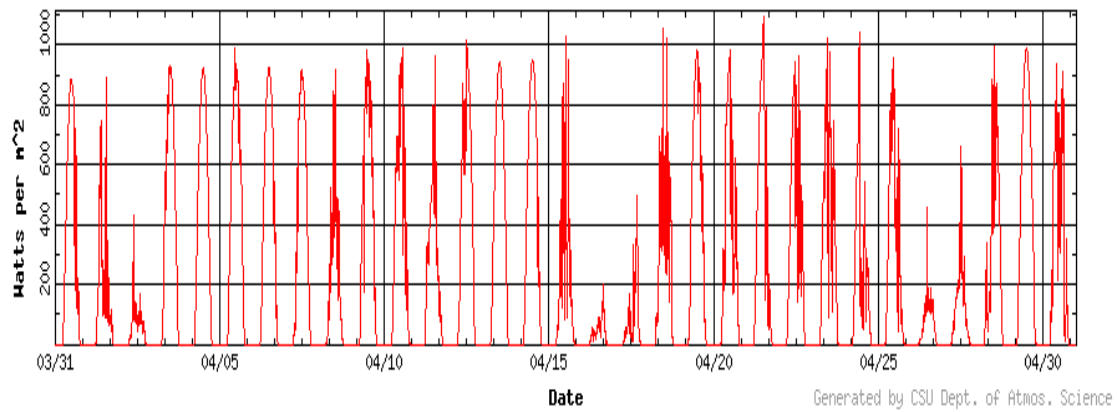


Figure A.20 Solar radiation April 2015

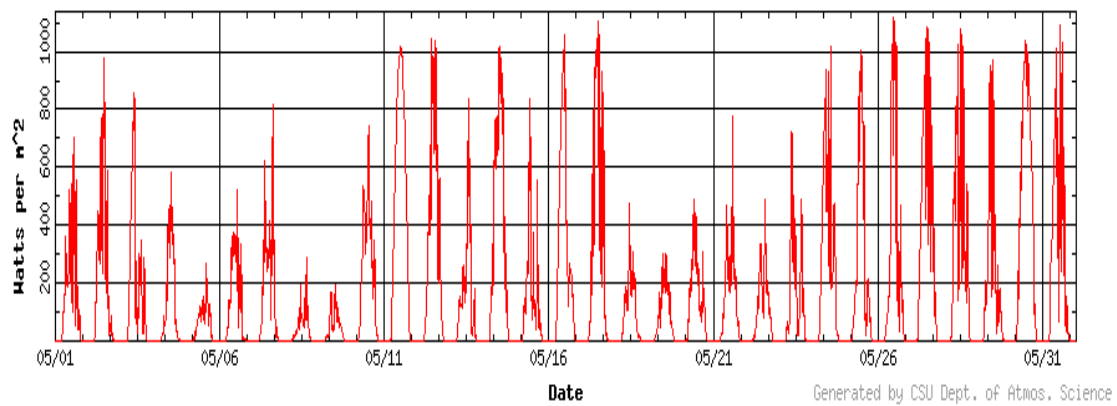


Figure A.21 Solar radiation May 2015

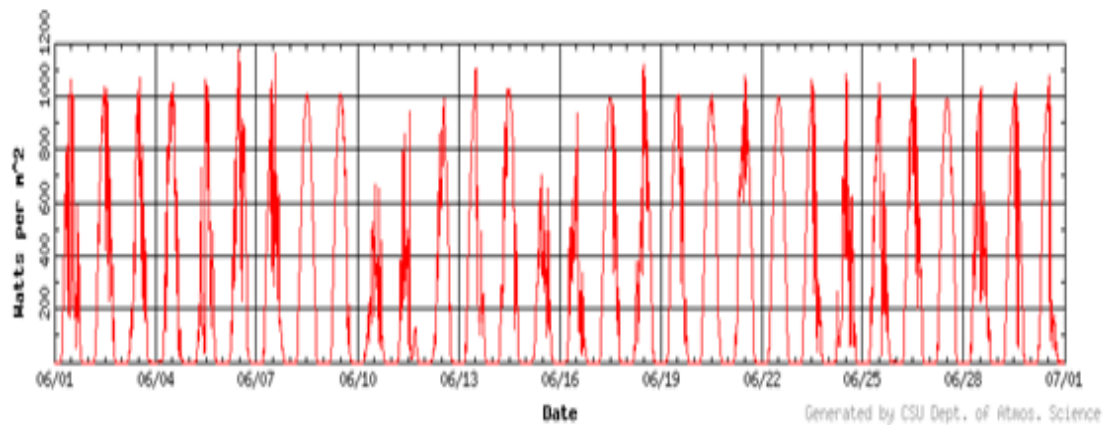


Figure A.22 Solar radiation June 2015

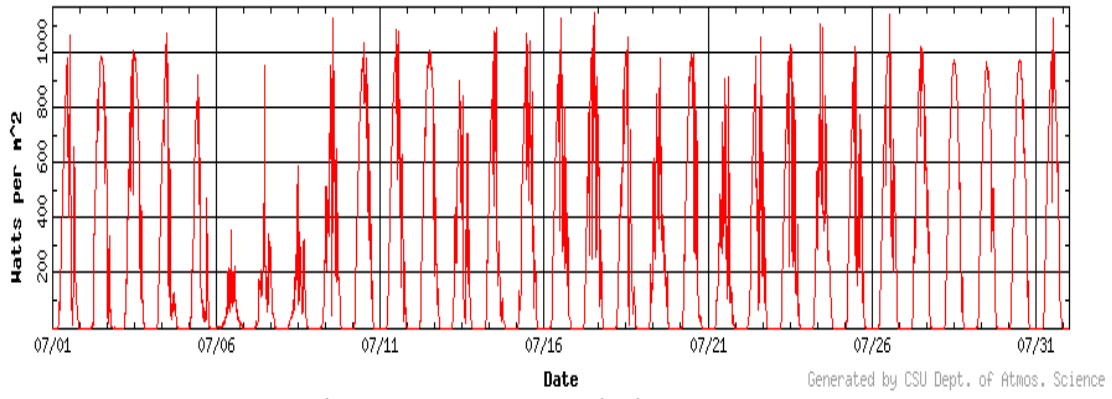


Figure A.23 Solar radiation July 2015

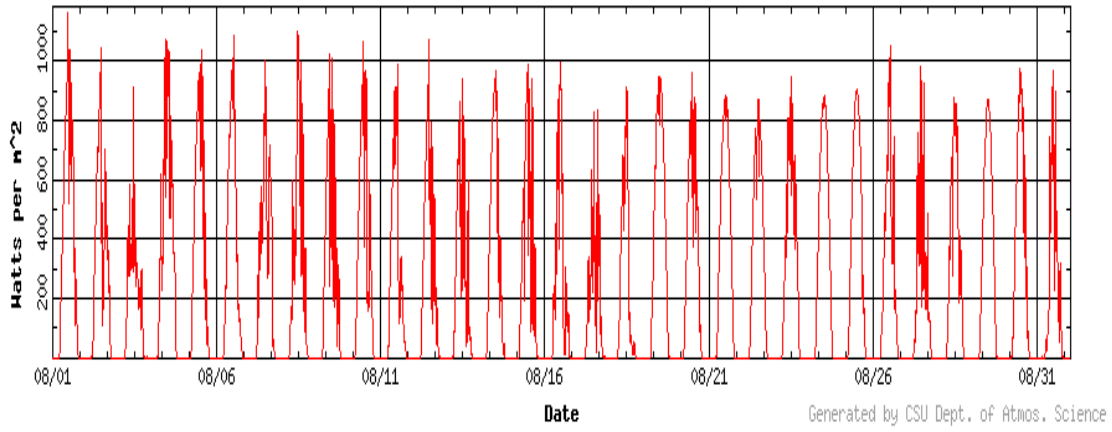
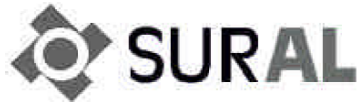


Figure A.24 Solar radiation August 2015

Appendix B

1. Conductor Datasheet



Avenida Francisco de Miranda, Edif. Parque Cristal, Torre Oeste
 Los Palos Grandes – Caracas 1062 - Venezuela
 Tel: +58 (212) 285-5707 Fax: +58 (212) 285-3269



PRODUCT CATALOG – ACSR (Aluminum Conductor, Steel Reinforced)

ASTM CONDUCTOR SIZES															
Code Word	Size (AWG or KCM)	Stranding (Al/St)	Diameter (inches)				Weight Per 1000 ft (Lbs)			Content %		Rated Strength (Lbs)	Resistance ¹ Ohms/1000 ft		Current Rating ² (Amps)
			Indiv. Al	Wires Stl	Steel Core	Complete Cable	Al	Stl	Total	Al	Stl		DC @ 20 °C	AC @ 75 °C	
Turkey	6	6/1	.0661	.0661	.0661	.198	24.5	11.6	36.1	67.90	32.10	1,190	.641	.806	105
Swan	4	6/1	.0834	.0834	.0834	.250	39.0	18.4	57.4	67.90	32.10	1,860	.403	.515	140
Swanate	4	7/1	.0772	.1029	.1029	.257	39.0	28.0	67.0	58.13	41.87	2,360	.399	.519	140
Sparrow	2	6/1	.1052	.1052	.1052	.316	62.0	29.3	91.3	67.90	32.10	2,850	.254	.332	184
Sparate	2	7/1	.0974	.1299	.1299	.325	62.0	44.7	106.7	58.13	41.87	3,640	.251	.338	184
Robin	1	6/1	.1181	.1181	.1181	.354	78.2	36.9	115.1	67.90	32.10	3,550	.201	.268	212
Raven	1/0	6/1	.1327	.1327	.1327	.398	98.7	46.6	145.3	67.90	32.10	4,380	.159	.217	242
Quail	2/0	6/1	.1489	.1489	.1489	.447	124.3	58.7	183.0	67.90	32.10	5,300	.126	.176	276
Pigeon	3/0	6/1	.1672	.1672	.1672	.502	156.7	74.0	230.7	67.90	32.10	6,620	.100	.144	315
Penguin	4/0	6/1	.1878	.1878	.1878	.563	197.7	93.4	291.1	67.90	32.10	8,350	.0795	.119	357
Waxwing	266.8	18/1	.1217	.1217	.1217	.609	250.3	39.2	289.5	86.45	13.55	6,880	.0643	.0787	449
Partridge	266.8	26/7	.1013	.0788	.2364	.642	251.7	115.6	367.2	68.53	31.47	11,300	.0637	.0779	475
Ostrich	300.0	26/7	.1074	.0835	.2505	.680	282.9	129.8	412.7	68.53	31.47	12,700	.0567	.0693	492
Merlin	336.4	18/1	.1367	.1367	.1367	.683	315.8	49.5	365.2	86.45	13.55	8,680	.0510	.0625	519
Linnet	336.4	26/7	.1137	.0884	.2652	.720	317.1	145.4	462.5	68.53	31.47	14,100	.0505	.0618	529
Oriole	336.4	30/7	.1059	.1059	.3117	.741	318.2	208.9	527.1	60.35	39.65	17,300	.0502	.0613	535
Chickadee	297.5	18/1	.1486	.1486	.1486	.743	373.1	58.5	431.6	86.45	13.55	9,940	.0432	.0529	576
Brant	397.5	24/7	.1287	.0858	.2574	.772	375.0	137.0	512.0	73.23	26.77	14,600	.0430	.0526	584
Ibis	397.5	26/7	.1236	.0961	.2883	.783	374.7	171.9	546.6	68.53	31.47	16,300	.0428	.0523	587
Lark	397.5	30/7	.1151	.1151	.3453	.806	375.8	246.8	622.6	60.35	39.65	20,300	.0425	.0519	594
Pelican	477.0	18/1	.1628	.1628	.1628	.814	447.8	70.2	518.0	86.45	13.55	11,800	.0360	.0442	646
Flicker	477.0	24/7	.1410	.0940	.2820	.846	450.1	164.4	614.5	73.23	26.77	17,200	.0358	.0439	655
Hawk	477.0	26/7	.1354	.1053	.3159	.858	449.6	206.4	656.0	68.53	31.47	19,500	.0356	.0436	659
Hen	477.0	30/7	.1261	.1261	.3783	.883	451.1	296.2	747.3	60.35	39.65	23,800	.0354	.0433	666
Osprey	556.5	18/1	.1758	.1758	.1758	.879	522.2	81.8	604.1	86.45	13.55	13,700	.0308	.0379	711
Parakeet	556.5	24/0	.1523	.1015	.3045	.914	525.1	191.7	716.9	73.23	26.77	19,800	.0307	.0376	721
Dove	556.5	26/7	.1463	.1138	.3414	.927	525.0	241.0	766.0	68.53	31.47	22,600	.0306	.0375	726
Eagle	556.5	30/7	.1362	.1362	.4086	.953	526.3	345.6	871.8	60.35	39.65	27,800	.0303	.0372	734
Peacock	605.0	24/7	.1588	.1059	.3177	.953	570.9	208.7	779.6	73.23	26.77	21,600	.0282	.0346	760
Squab	605.0	26/7	.1525	.1186	.3558	.966	570.4	261.8	832.2	68.53	31.47	24,300	.0281	.0345	765
Wood Duck	605.0	30/7	.1420	.1420	.4260	.994	572.0	375.6	947.7	60.35	39.55	28,900	.0279	.0342	774
Teal	605.0	30/19	.1420	.0852	.4260	.994	572.0	367.4	939.4	60.89	39.11	30,000	.0279	.0342	773
Kingbird	636.0	18/1	.1880	.1880	.1880	.940	597.2	93.6	690.8	86.45	13.55	15,700	.0270	.0332	773
Swift	636.0	36/1	.1329	.1329	.1329	.930	596.9	46.8	643.7	92.80	7.20	13,800	.0271	.0334	769
Rook	636.0	24/7	.1628	.1085	.3255	.977	600.0	219.1	819.1	73.23	26.77	22,600	.0268	.0330	784

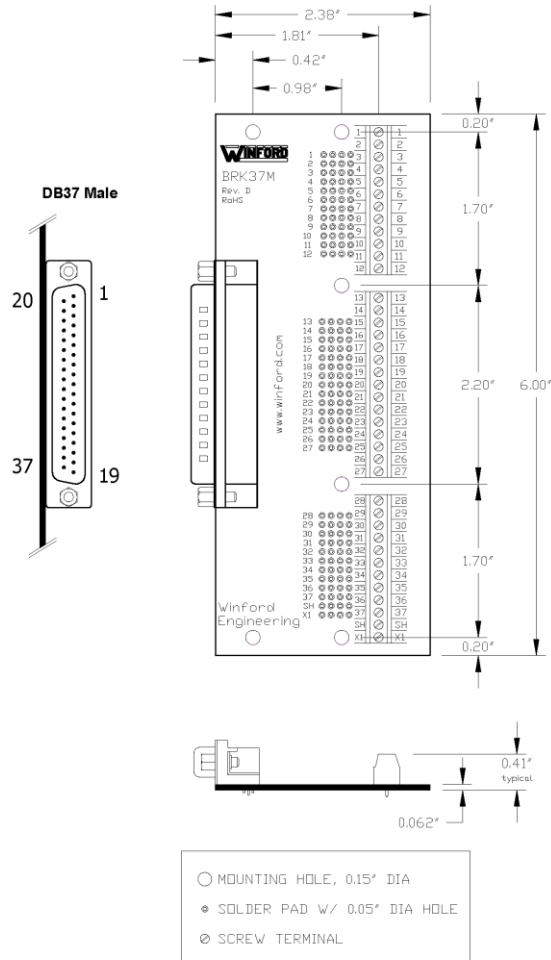
2. BRK37M breakout board



WINFORD ENGINEERING, LLC
4169 Four Mile Road • Bay City, MI 48706

Phone: 1-877-634-2673
FAX: 1-989-671-2941
www.winford.com

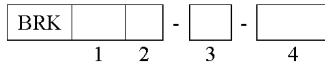
BRK37M Rev D Datasheet



BRK37M Rev D Specifications

Ambient Temperature	-20°C to 85°C
Ambient Humidity	10% to 90% RH, non-condensing
Voltage	200V maximum between any two signals
Continuous Current	1.5A maximum on any signal
Screw Terminal Size	Accepts 16 - 26 AWG wire

Part Number Ordering Information



1. Connector Positions

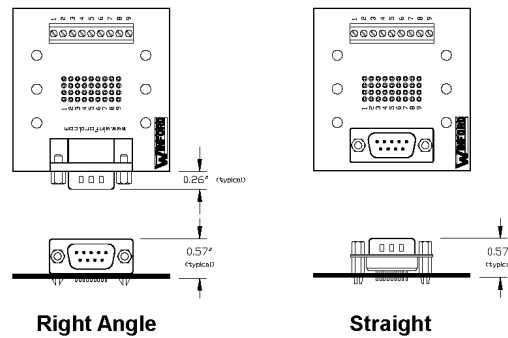
- **9** DB9
 - **15** DB15 (two-row)
 - **15HD** DB15 High Density (three-row)
 - **25** DB25
 - **37** DB37
- (more D-Sub varieties are also available)

2. Connector Gender

- **M** Male (Plug)
- **F** Female (Socket)

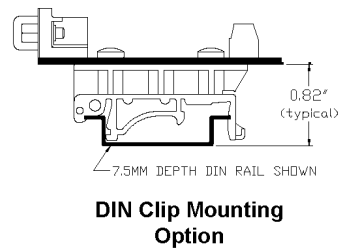
3. Connector Style

- **R** Right Angle
- **S** Straight (Vertical)



4. Mounting Option

- **FT** Rubber Feet on bottom side of PCB
- **DIN** DIN Rail Mounting Clips



TRITA TRITA-EE 2016:005